OXFORD JOURNALS
Forestry An International Journal of Forest Research

Satellite open data to monitor forest damage caused by extreme climate-induced events: a case study of the Vaia storm in Northern Italy

Journal:	*Forestry: An International Journal of Forest Research*
Manuscript ID	Forestry-2020-121.R2
Manuscript Type:	Original Article
Date Submitted by the Author:	n/a
Complete List of Authors:	VAGLIO LAURIN, Gaia; University of Tuscia, Francini, Saverio; University of Florence; Università degli Studi del Molise Dipartimento di Bioscienze e Territorio, Dipartimento di Bioscienze e Territorio, Luti, Tania; University of Florence Chirici, Gherardo; Universita degli Studi di Firenze, GESAAF Pirotti, Francesco; University of Padova, TESAF Papale, Dario; University of Tuscia
Keywords:	Forest damages, Windthrow, Remote Sensing, Sentinel 1, Sentinel 2

Forestry *An International Journal of Forest Research*

Institute of Chartered Foresters

Satellite open data to monitor forest damage caused by extreme climate-induced events: a case study of the Vaia storm in Northern Italy

Gaia Vaglio Laurin[1*], Saverio Francini[2,5], Tania Luti[3], Gherardo Chirici[2], Francesco Pirotti[4], Dario Papale[1]

[1] *Department for Innovation in Biological, Agro-Food and Forest Systems, University of Tuscia, Viterbo, 01100, Italy*

[2] *Department of Agricultural, Food and Forestry Systems, Università degli Studi di Firenze, Firenze, 50145, Italy*

[3] *Department of Earth Science, Università degli Studi di Firenze, Firenze, 50121, Italy*

[4] *Interdepartmental Research Center of Geomatics (CIRGEO), University of Padova, Legnaro, 35020, Italy*

[5] *Dipartimento di Bioscienze e Territorio, Università degli Studi del Molise, Pesche, Isernia, Italy*

*Corresponding author: Tel: +39 0761 357394; Fax: +39 0761 357389; Email: gaia.vl@unitus.it

The frequency of extreme storm events has significantly increased in the past decades, causing significant damage to European forests. To mitigate the impacts of extreme events a rapid assessment of forest damage is crucial, and satellite data are an optimal candidate for this task. The integration of satellite data in the operational phase of monitoring forest damage can be exploit the complementarity of optical and Synthetic Aperture Radar open datasets from the Copernicus programme. This study illustrates the testing of Sentinel 1 and Sentinel 2 data for the detection of areas impacted by the Vaia storm in Northern Italy. The use of multispectral Sentinel 2 provided the best performance, with classification Overall Accuracy values up to 86%; however optical data use are seriously hampered by cloud cover that can persist for months after the event and in most cases cannot be considered an appropriate tool if a fast response is required. The results obtained using Synthetic Aperture Radar Sentinel 1 were slightly less accurate (Overall Accuracy up to 68%), but the method was able to provide valuable information rapidly, mainly because the acquisition of this dataset is weather independent. Overall, for a fast assessment Sentinel 1 is the better of the two methods where multispectral and ground data are able to further refine the initial SAR-based assessment.

Introduction

In recent years, extreme climate-induced events have caused significant damage to European forests. The occurrence of strong storms has significantly increased in the past decades (Usbeck et al. 2010), and the frequency of these events is expected to increase further in future years due to changing climate dynamics (Saadet al. 2017; Seidl et al. 2014). Windthrow has a major impact on forest dynamics. Forests affected by repeated damage may not have enough time to recover and are more vulnerable to other threats. The forest regeneration in areas damaged by storms can alter the overall ecosystem succession, with consequences on biodiversity (Ellison et al. 2005). The way in which the windthrown timber is managed has an impact on biodiversity (Duelli et al. 2019). After a storm, the fungal infections over deadwood can increase and expand, promoting stand degradation (McCarthy et al. 2012); similarly, the expansion of outbreaks of bark beetles from damaged to healthy stands, that commonly occur from one to three years after windthrow, is known to additionally impact conifer forests (Havašová et al. 2017). Civil security issues can also be very relevant in windthrow areas (Gardiner et al. 2010).

Rapid assessment of forest damage is crucial for decision support regarding actions to be taken to prevent further damage and to mitigate the impacts of future extreme events. Field operations are commonly the first response from forest authorities for human security, timber management, and ecosystem conservation. The planning and execution of forest operations takes advantage from the availability of rapid information regarding spatial characteristics of the strongly impacted sites and also regarding the extent and severity of damage. Accessibility of remote forest areas is also a key factor that influences efforts that are required to collect this type of data. Remote sensing (RS) has frequently been employed to monitor different forest hazards and it has been previously used also in the case of the detection of storm-damaged trees. Various RS data can be used for post-event forest damage assessment, each having specific advantages and disadvantages, with their selection driven by site characteristics, imagery and resources availability, and the question being answered (Schwarz et al. 2003). Several case studies are needed, considering the variety of instruments and environmental conditions, to understand how to better support the integration of remote sensing tools in forest management practice.

With airborne or UAVs surveys, very detailed information up to single tree level can be produced using digital cameras (Duan et al. 2017; Hamdi et al. 2019; Honkavaara et al. 2013; Mokroš et al. 2017; Pirotti et al. 2016), or laser scanning instruments (Marchi et al. 2017; Chirici et al. 2018), or commercial multispectral sensors (Jackson et al. 2000). But on-demand airborne or UAVs surveys are costly, suited for areas of limited extent, and flights can be hampered for weeks after the event by bad weather conditions, such as heavy rain or post-fire smoke. Natural hazards often affect large areas and cause diffuse impacts, consequently the mapping and monitoring of the area can take advantage of the use of data from satellite platforms, that can cover broad extents repeatedly in time (Poursanidis and Chrysoulakis 2017). For this purpose, on-demand multispectral satellite images at very high spatial resolution (< 5 m) were previously successfully used in Russian (Kislov et al. 2020), and in German forests (Einzmann et al. 2017; Schwarz et al. 2003). Several forest damage assessments were conducted using medium spatial resolution multispectral data, particularly the Landsat open archive that offers free data at 30 m pixel size. As an example, with Landsat data an old diffusive windthrow caused by a storm was detected in a French forest by Haidu et al. (2019); disturbance due to intensive harvesting and strong windthrow was mapped in Western Siberia forests by Dyukarev et al. (2011); damage caused by a wind storm were assessed in Lithuania forests by Jonikavičius and Mozgeris (2013); windthrow disturbance was mapped in the temperate forest zone of European Russia and the southern boreal forest zone of the United States by Baumann et al. (2014). Recently, a Pan-European mapping of windthrow was generated through a model based on Landsat images, plus ancillary forest data from other satellites and national inventory data (Pecchi et al. 2019). Overall, optical-based studies have demonstrated the feasibility of detecting windthrow in forests using satellite images and that the accuracy of results depends mainly on the spatial and spectral resolutions of the datasets. However, the use of optical data for the rapid assessment of forest windthrows is not encouraged due to different factors, including the purchase cost and time in the case of on-demand images, and, importantly, the presence of clouds that in most cases persists for weeks after weather-related events and hamper the use of satellite data.

To cope with these limits, the use of Synthetic Aperture Radar (SAR) satellite data are recommended for a faster response. SAR data are independent from solar illumination and weather. They are therefore available right after the event only depending on the revisit time of the carrier, even when adverse weather conditions persist. Different SAR missions are available at present, each with specific configurations in terms of the frequency of the active signal, the polarization, and the spatial resolution. In forests, the energy backscattered by SAR systems at higher frequencies (e.g. X and C-band) mainly comes from the crowns and the upper forest strata, while at lower frequencies (e.g. L and P-bands) the contribution from branches and trunks increases, together with the signal penetration through the canopy (Solimini et al. 2016). The SAR backscatter is also influenced by the water content and the geometric features of the target object, thus in the case of forests by the moisture levels (in vegetation and soil) and the vegetation structure, including stem, branches and leaf characteristics and architecture (Woodhouse 2005). In severely damaged forest areas the geometric features suddenly change, as well as the surface roughness, making SAR data potentially suitable for forest damage assessment, and specifically for detection of windthrow (Eriksson et al. 2012). SAR datasets can bring additional and complementary information with respect to optical data (e.g. on canopy roughness, water content, and volume) (Green 1998). Few studies proved the value of SAR data in the context of detection of forest windthrows including: a multisensor based research conducted by Schwarz et al. (2003), who compared the results obtained with SAR data against those from optical data; the detection of areas affected by wind and insect outbreaks performed with L-band data (Tanase et al. 2018);

and the detection of windthrow in Germany and Switzerland based on Sentinel 1 C-band data (Rüetschi et al. 2019).

Considering the different characteristics of satellite data, their integration into operational forest monitoring after extreme events seeks to exploit the complementary features of optical and SAR data. At present, this is feasible using the Copernicus European satellite missions, specifically the Sentinel 1 C-band SAR data and the Sentinel 2 optical multispectral data (Drusch et al. 2012; Torres et al. 2012). More relevant, these datasets are also available as preprocessed products in Google Earth Engine (GEE), an integrated platform designed to empower not only traditional remote sensing scientists but also a wider audience with limited technical image processing skills (Gorelick et al. 2017). With its dense time series of optical and SAR data provided free, already preprocessed, the Copernicus datasets represent an optimal tool for the rapid assessment of land processes, including large scale forest damage and windthrow, as in this specific case study.

The Vaia storm hit the North-Eastern part of Italy on the 29th October 2018; with winds exceeding 200 km/h and strong rainfall it caused extensive forest damage in 494 municipalities, destroying or severely damaging forests of about 42,500 ha, with an estimated stock of fallen trees of 85 million of cubic metres (Chirici et el. 2019). The Copernicus Emergency Mapping system reports only about 4000 ha of damaged areas, about 10% of the affected area, due to cloud cover presence in the optical images used for mapping (data available at: https://emergency.copernicus.eu/mapping/list-of-components/EMSR334). Following the Vaia storm, the impacted regions assessed the forest damage by means of the integration of aerial photographs or very high-resolution optical satellite images with data from field surveys.

The present research tests Sentinel 1 and Sentinel 2 data for the detection of areas impacted by the Vaia storm. To classify healthy and damaged areas, different algorithms were evaluated , including a Bayesian Generalized Linear Model, a k-Nearest Neighbors approach, and Random Forest, using ground data provided by the regional authorities for model calibration and validation. Change detection approaches based on pre and post event image differencing were frequently used in previous research (Dalponte et al. 2020; Ruetschi et al. 2019; Tanase et al. 2018). In this work we evaluated the impact of algorithm selection on results, to support the selection of proper methods in operational forest monitoring. The present research expands on the common monitoring of forest windthrow based on optical data, which is ineffective in case of adverse atmospheric conditions, and it introduces testing of Sentinel 1 SAR C-band. Sentinel 2 optical data are here tested for the first time, according to our knowledge, in the context of the detection of forest damages by storms. Even if the sensitivity of SAR signal to forest damages was previously illustrated by various authors (Eriksson et al. 2012; Thiele et al. 2012; Ulander et al. 2005), only very few studies exploited SAR for windthrow mapping (Ruetschi et al. 2019; Tanase et al. 2018), possibly due to data complexities and limited access to user-friendly processing tools. Thus, the present study can be of help to understand how SAR can support forestry practice, also considering that these data and related tools are increasingly available by different space agencies, and preprocessed Sentinel 1 datasets are delivered by GEE.

The aim of this research is to contribute to forestry practice, developing knowledge useful to operational management to exploit satellite open-data, and defining a strategy for the rapid detection of forest damage and the further refinement of information. Remote sensing has great potential to cost-efficiently map storm-affected regions, but previous research has been somewhat limited, as Sentinel 2 imagery was not previously exploited with this aim; and Sentinel 1 was only partially examined. Thus, further investigation to assess the potential of integrating satellite open-data into forest practical workflows is needed. Here the focus is on open-data from the Copernicus programme, exploiting the GEE platform for fast processing, demonstrating that this approach can significantly support decision makers with remote sensing-based assessment of windthrow damaged areas.

Methods

Study area and ground data

The research was conducted in Northern Italy, in areas affected by the windthrow and included in two selected Sentinel-2 tiles for which ground truth data were made available by local administrations encompassing three regions: Friuli Venezia Giulia, Trentino Alto Adige, and Veneto (fig. 1). These regions host important forest resources, and different local agencies in charge of their census and management were involved in assessing the Vaia impacts. These data can also by found in open databases (Forzieri et al. 2020).

Insert fig.1

For the Trentino Alto Adige region, ground data for the Trento Autonomous Province were provided by the local forest service, and for the Autonomous Province of Bozen by the Province authority; in both cases the area of damaged forest were detected on the basis of photointerpretation of aerial orthophotos, and integrated with data from field surveys. Overall, in Trentino Alto Adige there were 1463 discrete areas, covering 5913 ha, and with a mean area of 4 ha. For the Friuli Venezia Giulia region, ground data on forest damage were provided by the local forest service using aerial orthophotos and ground surveys; there were 499 damaged areas for this region, covering 3693 ha, with mean area of 7.4 ha. For the Veneto region, the ground data were provided by the Veneto Agency for agriculture payments (AVEPA), who are responsible to provide economic help in case of natural disasters. AVEPA provided a shapefile of the affected areas based on photointerpretation of very high resolution orthophotos (20 cm spatial resolution) and SPOT 6/7 satellite pre and post event images at 1.5 m spatial resolution. The dataset included information on area borders and estimation of percentage of damaged trees in each area. In total, there were 1588 damaged areas detected in Veneto, covering 4020 ha, and having a mean surface of 2.5 ha.

The data provided for these Italian regions included 3550 polygons that identify any area affected by the windthrow. These polygons were filtered out to create a subset for testing and validation purposes, according to the following inclusion criteria: (i) polygons >2 ha, to include areas compatible with the spatial resolution and the detection capability of the remote sensing data used in this study; (ii) polygons in which the average terrain slope was below 20% in at least 85% of the surface, to exclude areas of unreliable SAR signal, according to distortion; (iii) for the Veneto region only, polygons in which the amount of damaged trees resulted > 80%, that were more than 40% of the total Veneto polygons; (iv) polygons included in two Sentinel tiles, to test the methods in the most affected area (3218 polygons). For classification purposes, polygons in forest not impacted by the Vaia storm were also drawn in proximity of the impacted polygons, by on-screen photointerpretation of post-event Google imagery.

In particular, the first criterion was guided by the imagery spatial resolution and allowed to retain the larger damaged areas. The second criterion was derived after exploring the SAR distortion masks based on local incidence angle. These maps are a by-product of SAR data processing, that was additionally performed as these layers are not included in the GEE available datasets. The maps indicated frequent distortions above the 20% slope; to facilitate the analysis using GEE data, this single threshold was selected. The third criterion was applied in Veneto, and was introduced due to the different ways the Italian regions assessed damage. In fact, it was noted that Trentino and Friuli Venezia Giulia reported only areas where damage was very significant, while Veneto Region also digitized areas that were partially impacted. The dataset was standardized by keeping only the polygons with damage degree above 80% in Veneto. The application of the mentioned criteria resulted in a standardized dataset including the larger and most affected areas, where SAR data had the higher signal to noise ratio and the forest impacts were similar. The damaged and non-damaged datasets included a total of 209 polygons, 104 from healthy forest stands, and 105 from damaged forest areas; the corresponding pixels were extracted from the imagery and averaged at polygon level. In total 90% of the 209 polygons were used to calibrate and validate with the k-fold approach classification algorithms. The remaining 22 polygons were used as independent test set for further evaluation of the overall accuracy. The total area used for calibration, validation and testing the methods was considerable: in Trentino Alto Adige it was equal to 622 ha; in Veneto to 533 ha; and in Friuli 237 ha, representing the different forest types and environmental conditions occurring in the area of interest.

Copernicus Sentinel data

The Sentinel 2 (S2) multispectral images were downloaded from Google Earth Engine as Level-2A orthorectified atmospherically corrected surface reflectance. The S2 Multispectral Instrument (MSI) samples 13 spectral bands: visible and NIR at 10 meters, red edge and SWIR at 20 meters, and atmospheric bands at 60 meters spatial resolution. Only bands at 10 - 20 m spatial resolution were used for tests (bands # 2, 3, 4, 5, 6, 7, 8, 8A, 11, 12), resampling at 10 m the 20 m bands with a nearest neighbor approach. The vegetation indices included in Table 1 were also computed.

Insert Table 1

To evaluate the hypothesis that Sentinel 2 data can detect the damaged forest areas with significant accuracy, post-event Sentinel 2 images were used. The possibility to use also a pre-damage image and focus the analysis on the variations in reflectance was also evaluated, but confounding factors such as day-specific atmospheric conditions, including cloud cover, and plant phenology stage at different dates were considered relevant causes of increased uncertainty in results and leading to uncertainty. Therefore, we preferred to work only on post-damage optical images using a binary classification approach (healthy forest/damaged areas).

The first available post-event Sentinel 2 imagery is dated June 2019 (7 months after the event). The predictor set named S2_Set1 (set of image bands) was used to evaluate the contribution of each single band, and the S2_Set2 (vegetation indices) to evaluate the contribution of the derived vegetation indices. The latter combination is preferable in case different images are used (predictor sets in Table 2).

The Sentinel 1 SAR images were downloaded from Google Earth Engine as Ground Range Detected (GRD) scenes, already pre-processed using the Sentinel-1 Toolbox to generate a calibrated, ortho-corrected product at 10 m spatial resolution in dual-band cross polarization mode (VV – VH). Preprocessing included thermal noise removal, radiometric calibration, and terrain correction using a digital terrain model (SRTM 30 m). Five pre-event scenes were collected from the period 26 September - 3 October 2018 (pre-event period without frost or snow), and 5 post-event scenes were from the period 7 - 15 December 2018. The pre and post event scenes were averaged at pixel level, and band ratios (VV/VH, VH/VV), and band normalized differences were also computed (VV-VH, VH -VV). In fact, with respect to the optical images, the SAR data are less affected by atmospheric condition and vegetation phenology and for this reason the use of differences between pre and post event was also evaluated to detect forest damaged areas.

Thus, the set of predictors named S1_Set3 (based only on post-event bands), and the S1_Set4 (based on pre-post event scenes differences) were used in tests (predictor sets in Table 2).

Insert Table 2

Classification approaches

Three different approaches were tested for the classification task: a generalized linear Bayesian model and two machine learning models, the k-Nearest Neighbors and Random Forest. Using the three models and the four sets of available predictors (Table 2), a total of 12 models-predictors combinations were developed. The tests were conducted using the RFTrainer, KNN, and Bayesglm R packages in R environment (R Core Team 2013).

Bayesian inference is a method of statistical inference in which Bayes' theorem is used to update the probability for a hypothesis as more evidence or information becomes available. It facilitates representing and taking full account of the uncertainties related to models and parameter values. The Bayesian generalized linear model (BGLM) is based on Bayesian functions that finds an approximate posterior mode and variance using extensions of the classical generalized linear model computations. The Bayesian function allows the user to specify independent prior distributions for the coefficients in the t family, with the default being Cauchy distributions with center 0 and scale set to 10 (for the regression intercept), 2.5

(for binary predictors), or 2.5/(2 · sd), where sd is the standard deviation of the predictor in the data (for other numerical predictors) (Berrett and Calder 2016; Gelman et al. 2008)

The k-Nearest Neighbors (KNN) technique is a popular method for producing spatially contiguous predictions of forest attributes by combining field and remotely sensed data. KNN are appealing as they can be used for both univariate and multivariate prediction, no assumptions regarding the distributions of response or auxiliary variables are necessary and they can be used with a wide variety of datasets (Chirici et al 2016). The k nearest vectors, used to perform the classification, are found according to Minkowski distance and the classification is performed by means of the maximum of summed kernel densities; both ordinal and continuous variables can be predicted (Wu et al. 2002).

Random Forest (RF) is an ensemble of decision trees that learns through a supervised approach and produces multiple models that are aggregated, using a bootstrap aggregating procedure, to produce the result. The models are built using different training subsets, generated by bootstrapping, that are used to build the “forest”. RF is able to reduce the output variance and the overfitting problem with respect to other machine learning approaches, improving model stability and accuracy (Breiman 2001).

When a model is trained with data there is the risk of overfitting, i.e. that the parameters are estimated to reproduce closely the training data used, losing the capacity to generalize outside the calibration examples. To avoid overfitting one of the most useful method is k-fold cross validation (k-fold CV) that splits the training set into K number of subsets, called folds: the models are then iteratively fitted K times each time training the data on data from K-1 of the folds and evaluating the performances on data from the Kth fold. At the end of calibration, the performance on each of the K folds are evaluated in term of Overall Accuracy (OA), i.e. the percentage of cases where the classification as damaged or not damaged was correct. The Overall Accuracy from Cross Validation - OA_{cv} and the relative standard deviation $sd(OA_{cv})$ are finally computed averaging the K folds and calculating their standard deviation. This provides more information over how stable the model is by testing it over multiple sets of data.

RF and kNN models require the calibration of hyperparameters- The hyperparameters are calculated using the training datasets. BGLM instead does not require hyperparameters calibration. A procedure based on a random search grid was used for the optimization (Bergstra and Bengio, 2012). The procedure defines a grid of hyperparameter ranges, as those defined above. One hundred combinations were randomly sampled from the grid and for each combination a k-Fold CV was performed. For both KNN and RF the optimal hyperparameters combination with the greater OA_{cv} was finally selected. In the RF case, the hyperparameters that were tuned include the maximum depth of each tree (max_depth) in the forest and the number of features (max_features) considered by each tree when splitting a node. The number of trees in the forest was set equal to 400, while the minimum number of samples required to split an internal node was set equal to 1.

In the kNN case the three hyperparameters that were optimized are: the number of neighbours considered (k), the Minkosky distance, and the kernel to use. The max_features ranged between 2 and n, where n equals the number of predictors used in input; the max_depth ranges between 1 and 40. k ranged between 1 and 60, the Minkosky distance was equal to the Euclidean and Manhattan distances, and the kernel to use were Unweighted, Weighted, Inverse, Reciprocal.

The models, once optimized and validated with k-fold approach, were further independently evaluated in terms of accuracy using the test set that includes 10% of the polygons never used during the optimization procedure. For the evaluation of the classification results, different statistics are reported, including overall accuracy, users accuracy, producers accuracy, and the percentage of omission and commission errors. User's accuracy represents how reliable the classification is in terms of actually finding damage in the real world over an area that was classified as “damaged” in the map. Producer's accuracy reports how often a damage that is found in the real world is reported in the final classified map (Cohen 1968; Congalton 1991).

Results

In table 3 we present for each model and for each of the four sets of predictors the averaged OA_{cv} obtained with a 9-fold cross validation procedure and the related standard deviation obtained averaging the different iterations. For the KNN and RF models the best hyperparameters combination, identified using a RandomSearch algorithm are also presented.

Insert Table 3

The results in Table 3, also graphically shown in fig. 2, show consistency in different models, with negligible differences among the considered approaches and limited variance from different iterations.

The best results are obtained with S2 images, with OA_{cv} always > 0.8 and included in the 0.8-0.85 range for either bands or vegetation indices, with the latter reaching a slightly higher accuracy. The standard deviation values resulted were always small with a maximum value of 0.102. This confirms the ability of S2 to detect impacted forest areas.

Lower accuracy results –in the 0.6-0.7 OA_{cv} range- are obtained when using SAR data with a slightly better scores obtained when using the S1_Set3, that includes only data from post-event scene.

Insert fig. 2

The three models were also applied to the independent test set (n = 22) to evaluate their final performance on new and unseen data and the results are shown in Table 4.

Insert Table 4

The results obtained using the independent test set are similar to those obtained with 9-fold CV but span, as expected, over a slightly higher range, considering the limited number of samples in the test set (n=22).

For sets 1 and 2, based on S2 data, the accuracy is included in the 0.77-0.86 range, and is similar across the three different models. For sets 3 and 4, based on S1 data, the accuracy range is 0.5-0.68, with higher results obtained using Random Forest model.

Overall, results in Table 4 confirm the higher accuracies obtained with the use of Sentinel 2 data with respect to those obtained with SAR data.

Discussion

The availability of satellite open-data that is also partly preprocessed adds significant value to the procedure of the assessment of forest damages, from windthrow or other sources of damage that change the landscape. The final product is a classified damage map that supports rapid responses in terms of forest management. The results indicate that data from the Copernicus Sentinel 1 and 2 missions are suited for the detection of damaged forest areas. SAR is especially useful for a fast evaluation, providing useful information for immediate/short-term response actions for risk mitigation. Sentinel 2 can be used to refine the SAR initial information unless post event data are immediately available. The use of cloud-based platforms like Google Earth Engine helps to reduce the time that operators need for image download and standard pre-processing. A pre-defined workflow over ready-to-use imagery can avoid requiring highly skilled operators for processing imagery. The workflow can be partly automatic, providing maps useful to multiple end-users, even those less familiar with image processing techniques.

Focusing on applications, the present research suggests that the sequential use of GEE Sentinel 1 and 2 data for better windthrow information provision is an optimal combination. Specifically, the testing of the different predictors from S1 and S2 data provided useful insights on the advantages and limits of these datasets.

The best detection of the forest areas impacted by the Vaia storm is always obtained using Sentinel 2 images. Using a 9-fold cross validation approach and either S2 bands or vegetation indices as input, the obtained overall accuracies were > 80%, with limited differences among modeling approaches, low variance from iterations, and results included in the 80-85% range. The use of vegetation indices with KNN and RF approaches provided the higher OA_{CV} values, equal to 85 and 84 %, respectively.

Very similar results are obtained when the parameterized models were validated against the independent test set, represented by 22 samples not used to calibrate the models. The obtained results, although the number of test samples is relatively low, are in a very similar OA range (77- 86%) compared with those reported for 9-fold cross validation. The highest OA score (86%) is obtained either using S2 bands with KNN model or using VIs with Random Forest. User accuracies were over 90% whereas producer's accuracies were in the 71-83% range, with higher scores obtained with RF and VIs. This indicates that commission errors where lower then omission errors, in other words some damaged areas where not correctly detected by the classifier, thus leaving out some areas from the final map, but most of the areas classified as damaged where really damaged. It might be due to canopy of felled trees still significantly showing in the image, or also reflectance from water vapor, that commonly rises in the morning in mountainous areas, mixing with the reflectance values from the tree trunks.

It should be considered that the post-event S2 imagery employed in the study were from a single date and about 7 months after the Vaia event. The time gap between the storm and the S2 imagery allows the greening of the ground in damaged areas, from herbal and shrubs vegetation regrowth that can produce a change in reflectance values and a consequent negative impact in the classification accuracy. The results are however in line with what has been already found in the past with Landsat data, thus at 30 m spatial resolution (30 m): an OA equal to 86% was reached in the detection of windthrows in Voges mountains in France (Haidu et al. 2019); in European Russia and United States the OA was about 75%, with more accurate results reported for larger areas (Baumann et al. 2014); and with an automatic algorithm based on Landsat time series, historical disturbance from windthrow and logging was detected in United States forest with an accuracy about 80%. According to our knowledge, there are no studies based on the use of S2 data for forest windthrow detection, except two abstracts where the accuracy of the obtained results is not reported (Cenci et al. 2019; Valt et al. 2019).

Vegetation indices are especially useful when multiple images are used (as in the case of change detection analysis), or when the study area is large and covered by different image tiles, or even when a mosaic from different dates is composed to mitigate cloud cover issues. In fact, VIs are designed to maximize sensitivity to the vegetation characteristics while minimizing confounding factors such as soil background reflectance, directional, or atmospheric effects, that change among different acquisitions (Fang and Liang 2008). According to this and based on the reported classification results, the use of VIs from S2 data, fitting the model with the RF method, appears the best solution to detect damaged forest area in this case study. An improvement in accuracy is expected if optical imagery becomes available in dates close to the time of the damage event.

The use of SAR inputs produced lower accuracies compared to S2 inputs with an OA values in the range 0.66-0.71 according to 9-fold cross validation and a low standard deviation score (< 0.14). Differences among the three models are minor, as well as those when using post-event data only or pre-post event backscattering difference. The highest OA_{cv} score is obtained with pre-event data and KNN approach (OA_{cv} = 0.71).

According to results from the independent test set, the OAs slightly decrease and the variability in values increases, being included in the 0.5-0.68 range. The best scores are obtained using RF: 64% and 68% in OA with post-event data and pre-post event difference, respectively. With RF, the user's accuracy is low (54%) when using S1 pre-post event scenes differences, but the producer's accuracy is in line with the one obtained using the S2 data (75%). When using post-event data, the user's and producer's accuracies are on the same order (63%). The results suggest the use of RF as classification model, and the combination of pre- and post-event SAR scenes to better meet the user's needs.

Previous studies conducted with C-band ERS 1/2 and RADARSAT 1 at 30 m spatial resolution were not successful for the detection of forest windthrows (Schwarz et al. 2003; Ulander et al. 2005). However, with L-band data - that better penetrates into the forest - OAs included in the 69-84% range were obtained in the Bavarian Forest National Park, with accuracy values depending on the acquisition date and environmental conditions (Tanase et al. 2018). Using C-band S1 and a change detection approach, the producer's accuracy reached 88% in a German validation site, but the user's accuracy was quite low (21%) and limitations consisted in a minimum area of 0.5 ha and the requirement of 10 post-event images (Rüetschi et al. 2019). Positive results were also obtained using X-band data with very high spatial resolution (Thiele et al. 2012).

The results here presented outline the relevance of SAR spatial resolution for forest windthrow detection, and confirm the ability of S1 data to produce fast preliminary information on impacted areas, with the obtained OA and user's accuracy included in a range of values similar to those reported by other studies.

It is important to note the limitations of the present study in terms of suitability in certain cases. First, the areas tested were all above 2 ha, to cope with the 10 m spatial resolution of both S1 and S2 datasets; however the average size of damaged areas in the three considered regions resulted higher than 2 ha. Then, the ground truth was filtered out to exclude slopes using a low threshold (> 20°) where the first SAR distortion effects were observed. Producing the distortion masks to filter out data, instead of a fixed threshold that excluded most slopes for easiness of analysis in GEE, could results in a detailed mapping of unreliable SAR pixels and a larger availability of reliable data over slopes. Similarly, the use of temporal series can improve the amount of area with reliable SAR data, as at each pass the acquisition angle may vary. When SAR data are used, it is also important to detect and mask pixels with wet or dry snow over the canopy, as it changes the backscatter values (Koskinen et al. 1997). This implies an added complexity of the method in areas seasonally covered by snow.

For future operational use, the application of a pre-disturbance forest/non-forest map can help to perform semi-automatic classification. Further tests are also needed to understand the response of satellite data over less impacted forests, where a mixture of healthy and damaged trees is present, and how to minimize the impact of SAR distortion areas.

The combined use of S1 and S2 was not investigated here, as for data integration the optical and radar imagery should be from same period. The S2 images used in this investigation were dated months after the storm, when the herbal and shrub vegetation renovation influence both the optical reflectance and the backscattering in C-band SAR. These are confounding factors, but a data integration approach is feasible if optical data are available soon after the event. Higher accuracy in classification is known to occur from combining SAR with optical with respect to use single sensor type (Clerici et al. 2017; Vaglio Laurin et al. 2012), so this might be another strategy to improve the information accuracy.

Conclusion

This study showed the suitability of Copernicus S1 and S2 data for the detection of areas affected by windthrow. Sentinel 2 provided the best performance for detection of windthrow areas, but its use was seriously hampered by cloud cover. For events occurring in winter, Sentinel 2 data might only be available after several months. In those cases, the use of Sentinel 1 data, being independent with respect to atmospheric condition and with a fast return time, becomes the best option for a first and rapid evaluation of the forest damage, to support field operations and the formation of management response plans.

Thus, for operational monitoring, the results suggest a sequential approach, based initially on S1 for fast response. This initial SAR assessment can be refined in later dates, integrating S2 imagery when available and data from ground or aerial surveys, for a more accurate mapping also over steep slopes.

Data availability statement

Remote sensing data are freely available by the Copernicus facilities. Ground data were provided by local authorities and can be requested directly to them. Part of the data can be found in the open database published by Forzieri et al. (2020).

Funding

This work was supported by internal resources of the participating institutes. In particular F.P.'s work was supported by University of Padova's VAIA-FRONT (VAIA, FROm lessons learNT to future options) project.

Acknowledgements

For the Trentino Autonomous Province, we acknowledge Dr. A. Wolynski from the local forest service who coordinated the acquisition of ground data on the basis of aerial photography and field surveys.

For the Alto Adige region, we acknowledge Dr. F. Maistrelli from the Autonoumous Province of Bozen who provided the ground data delimitated on the basis of aerial photography and field surveys.

For the Friuli Venezia Giulia region, we acknowledge Dr. R. Comino from the local forest service who coordinated the acquisition of ground data on the basis of aerial photography and ground surveys.

For the Veneto Region we acknowledge the Agenzia Veneta per i Pagamenti in Agricoltura (AVEPA) that provided the data.

Conflict of interest statement

'None declared.'

References

Baumann, M.; Ozdogan, M.; Wolter, P.T.; Krylov, A.; Vladimirova, N.; Radeloff, V.C. (2014) Landsat remote sensing of forest windfall disturbance. Remote Sens. Environ., 143, 171–179.

Bergstra, J., & Bengio, Y. (2012). Random search for hyper-parameter optimization. Journal of machine learning research, 13, 281-305.

Berrett, C., & Calder, C. A. (2016). Bayesian spatial binary classification. Spatial Statistics, 16, 72-102.

Breiman, L. (2001). Random forests. Machine learning, 45(1), 5-32.

Cenci, L., De Giorgi, A., Squicciarino, G., Pulvirenti, L., Moser, G., & Boni, G. (2019). Exploiting Sentinel 2 data for mapping windstorm damages in forested areas. Case Study: the event of October 2018 occurred in Northeast Italy. *Geophysical Research Abstracts*, vol. 21.

Chirici, G., Mura, M., McInerney, D., Py, N., Tomppo, E. O., Waser, L. T., ... & McRoberts, R. E. (2016). A meta-analysis and review of the literature on the k-Nearest Neighbors technique for forestry applications that use remotely sensed data. Remote Sensing of Environment, 176, 282-294.

Chirici, G., Bottalico, F., Giannetti, F., Del Perugia, B., Travaglini, D., Nocentini, S., ... & Fattorini, L. (2018). Assessing forest windthrow damage using single-date, post-event airborne laser scanning data. Forestry: An International Journal of Forest Research, 91(1), 27-37.

Chirici, G., Giannetti, F., Travaglini, D., Nocentini, S., Francini, S., D'Amico, G., ... & Tonner, J. (2019). Stima dei danni della tempesta "Vaia" alle foreste in Italia. Forest@-Journal of Silviculture and Forest Ecology, 16(1), 3.

Clerici, N., Valbuena Calderón, C. A., & Posada, J. M. (2017). Fusion of Sentinel-1A and Sentinel-2A data for land cover mapping: a case study in the lower Magdalena region, Colombia. Journal of Maps, *13*(2), 718-726.

Cohen, J. (1968) Weighted kappa: Nominal scale agreement with provision for scaled disagreement or partial credit. Psychological Bulletin 70 (4):213-220.

Congalton, R.G. (1991) A review of assessing the accuracy of classification of remotely sensed data. Remote Sensing of Environment 37:35-46

Dalponte, M., Marzini, S., Solano-Correa, Y. T., Tonon, G., Vescovo, L., & Gianelle, D. (2020). Mapping forest windthrows using high spatial resolution multispectral satellite images. International Journal of Applied Earth Observation and Geoinformation, 93, 102206.

Drusch, M., Del Bello, U., Carlier, S., Colin, O., Fernandez, V., Gascon, F., ... & Meygret, A. (2012) Sentinel-2: ESA's optical high-resolution mission for GMES operational services. Remote sensing of Environment, 120, 25-36.

Duan, F.; Wan, Y.; Deng, L. (2017) A novel approach for coarse-to-fine windthrown tree extraction based on unmanned aerial vehicle images. Remote Sens., 9, 306.

546 Duelli, P., Wermelinger, B., Moretti, M., & Obrist, M. K. (2019). Fire and windthrow in
547 forests: Winners and losers in Neuropterida and Mecoptera. Alpine Entomology, 3, 39.

548 Dyukarev, E.A.; Pologova, N.N.; Golovatskaya, E.A.; Dyukarev, A.G. (2011) Forest cover
549 disturbances in the South Taiga ofWest Siberia. Environ. Res. Lett., 68.

550 Einzmann, K., Immitzer, M., Böck, S., Bauer, O., Schmitt, A., & Atzberger, C. (2017)
551 Windthrow detection in European forests with very high-resolution optical data. Forests, 8(1),
552 21.

553 Ellison, A. M. et al. (2005) Loss of foundation species: Consequences for the structure and
554 dynamics of forested ecosystems. Front. Ecol. Environ. 3, 479–486.

555 Eriksson, L.E.B.; Fransson, J.E.S.; Soja, M.J.; Santoro, M. (2012) Backscatter signatures of
556 wind-thrown forest in satellite SAR images. In Proceedings of the International Geoscience
557 and Remote Sensing Symposium (IGARSS), Munich, Germany, 22–27 July; pp. 6435–6438.

558 Fang H. and S. Liang. (2008) Leaf Area Index Models. Encyclopedia of Ecology, pp. 2139-
559 2148

560 Forzieri, G., Pecchi, M., Girardello, M., Mauri, A., Klaus, M., Nikolov, C., … Beck, P. S. A.
561 (2020). A spatially explicit database of wind disturbances in European forests over the period
562 2000 - 2018. Earth System Science Data, 12(1), 257–276.

563 Gardiner, B., Blennow, K., Carnus, J. M., Fleischer, P., Ingemarsson, F., Landmann, G., ... &
564 Peyron, J. L. (2010). Destructive storms in European forests: past and forthcoming impacts.
565 European Forest Institute, Efiatlantic.

566 Gelman, A., Jakulin, A., Pittau, M. G., & Su, Y. S. (2008) A weakly informative default prior
567 distribution for logistic and other regression models. The annals of applied statistics, 2(4),
568 1360-1383.

569 Gorelick, N., Hancher, M., Dixon, M., Ilyushchenko, S., Thau, D., & Moore, R. (2017)
570 Google Earth Engine: Planetary-scale geospatial analysis for everyone. Remote sensing of
571 Environment, 202, 18-27.

572 Green, R.M. (1998) The sensitivity of SAR backscatter to forest windthrow gaps. Int. J.
573 Remote Sens., 19, 2419–2425.

574 Haidu, I., Furtuna, P. R., & Lebaut, S. (2019) Detection of old scattered windthrow using low
575 cost resources. The case of Storm Xynthia in the Vosges Mountains, 28 February 2010. Open
576 Geosciences, 11(1), 492-504.

577 Hamdi, Z. M., Brandmeier, M., & Straub, C. (2019) Forest Damage Assessment Using Deep
578 Learning on High Resolution Remote Sensing Data. Remote Sensing, 11(17), 1976.

Havašová, M., Ferenčík, J., & Jakuš, R. (2017) Interactions between windthrow, bark beetles and forest management in the Tatra national parks. Forest Ecology and Management, 391, 349-361.

Honkavaara, E.; Litkey, P.; Nurminen, K. (2013) Automatic Storm Damage Detection in Forests Using High-Altitude. Photogrammetric Imagery. Remote Sens., 5, 1405–1424.

Huang, C., Goward, S. N., Masek, J. G., Thomas, N., Zhu, Z., & Vogelmann, J. E. (2010) An automated approach for reconstructing recent forest disturbance history using dense Landsat time series stacks. Remote Sensing of Environment, 114(1), 183-198.

Jackson, R. G., Foody, G. M., & Quine, C. P. (2000) Characterizing windthrown gaps from fine spatial resolution remotely sensed data. Forest Ecology and Management, 135(1-3), 253-260.

Jonikavičius, D., & Mozgeris, G. (2013) Rapid assessment of wind storm-caused forest damage using satellite images and stand-wise forest inventory data. iForest-Biogeosciences and Forestry, 6(3), 150.

Kislov, D. E., & Korznikov, K. A. (2020) Automatic Windthrow Detection Using Very-High-Resolution Satellite Imagery and Deep Learning. Remote Sensing, 12(7), 1145.

Koskinen, J.T.; Pulliainen, J.T.; Hallikainen, M.T. (1997) The Use of ERS-1 SAR Data in Snow Melt Monitoring. IEEE Trans. Geosci. Remote Sens. 35, 601–610.

Marchi, N., Pirotti, F., & Lingua, E. (2018). Airborne and Terrestrial Laser Scanning Data for the Assessment of Standing and Lying Deadwood: Current Situation and New Perspectives. Remote Sensing, 10(9), 1356.

McCarthy, J. K., Hood, I. A., Kimberley, M. O., Didham, R. K., Bakys, R., Fleet, K. R., ... & Brockerhoff, E. G. (2012) Effects of season and region on sapstain and wood degrade following simulated storm damage in Pinus radiata plantations. Forest ecology and management, 277, 81-89.

Mokroš, M.; Výbošt'ok, J.; Merganicˇ, J.; Hollaus,M.; Barton, I.; Korenˇ ,M.; Tomaštík, J.; Cˇ ernˇava, J. (2017) Early stage forest windthrow estimation based on unmanned aircraft system imagery. Forests 8, 306.

Pecchi, M., Forzieri, G., Ceccherini, G., Spinoni, J., Feyen, L., Cescatti, A., & Chirici, G. (2019) Pan-European mapping of windthrows. Geophysical Research Abstracts, vol. 21.

Pirotti, F., Travaglini, D., Giannetti, F., Kutchartt, E., Bottalico, F., & Chirici, G. (2016). Kernel feature cross-correlation for unsupervised quantification of damage from windthrow in forests. ISPRS - International Archives of the Photogrammetry, Remote Sensing and Spatial Information Sciences, XLI-B7, 17–22.

Poursanidis, D., & Chrysoulakis, N. (2017) Remote Sensing, natural hazards and the contribution of ESA Sentinels missions. Remote Sensing Applications: Society and Environment, 6, 25-38.

R Core Team (2013). R: A language and environment for statistical computing. R Foundation for Statistical Computing, Vienna, Austria. URL http://www.R-project.org/.

Rüetschi, M., Small, D., & Waser, L. T. (2019) Rapid detection of windthrows using sentinel-1 c-band sar data. Remote Sensing, *11*(2), 115.

Saad, C., Boulanger, Y., Beaudet, M., Gachon, P., Ruel, J. C., & Gauthier, S. (2017) Potential impact of climate change on the risk of windthrow in eastern Canada's forests. Climatic Change, 143(3-4), 487-501.

Schwarz, M., Steinmeier, C., Holecz, F., Stebler, O., & Wagner, H. (2003) Detection of windthrow in mountainous regions with different remote sensing data and classification methods. Scandinavian journal of forest research, 18(6), 525-536.

Seidl, R., Schelhaas, M. J., Rammer, W., & Verkerk, P. J. (2014) Increasing forest disturbances in Europe and their impact on carbon storage. Nature climate change, 4(9), 806-810.

Solimini, D. (2016) Understanding Earth Observation; Springer International Publishing: Basel, Switzerland, pp. 1–703, ISBN 978-3-319-25633-7.

Tanase, M. A., Aponte, C., Mermoz, S., Bouvet, A., Le Toan, T., & Heurich, M. (2018) Detection of windthrows and insect outbreaks by L-band SAR: A case study in the Bavarian Forest National Park. Remote Sensing of Environment, 209, 700-711.

Thiele, A., Boldt, M., & Hinz, S. (2012) Automated detection of storm damage in forest areas by analyzing TerraSAR-X data. In: 2012 IEEE International Geoscience and Remote Sensing Symposium (pp. 1672-1675). IEEE.

Torres, R.; Snoeij, P.; Geudtner, D.; Bibby, D.; Davidson, M.; Attema, E.; Potin, P.; Rommen, B.Ö.; Floury, N.; Brown, M.; et al. (2012) GMES Sentinel-1 mission. Remote Sens. Environ., 120, 9–24.

Ulander, L.M.H.; Smith, G.; Eriksson, L.; Folkesson, K.; Fransson, J.E.S.; Gustavsson, A.; Hallberg, B.; Joyce, S.; Magnusson, M.; Olsson, H.; et al. (2005) Mapping of wind-thrown forests in southern Sweden using space- and airborne SAR. In Proceedings of the International Geoscience and Remote Sensing Symposium (IGARSS), Seoul, South Korea, 25–29 July 2005; pp. 3619–3622.

Usbeck, T., Wohlgemuth, T., Dobbertin, M., Pfister, C., Bürgi, A., & Rebetez, M. (2010). Increasing storm damage to forests in Switzerland from 1858 to 2007. Agricultural and Forest Meteorology, 150(1), 47-55.

Vaglio Laurin, G., Liesenberg, V., Chen, Q., Guerriero, L., Del Frate, F., Bartolini, A., ... & Valentini, R. (2013) Optical and SAR sensor synergies for forest and land cover mapping in a tropical site in West Africa. International Journal of Applied Earth Observation and Geoinformation, 21, 7-16.

Valt, M., Salvatori, R., & Salzano, R. (2019) Mapping the effects of VAIA storm using Sentinel 2 data. *Geophysical Research Abstracts,* vol. 21.

Woodhouse, I. H. (2005). Introduction to microwave remote sensing. CRC press.

Wu, Y., Ianakiev, K., & Govindaraju, V. (2002) Improved k-nearest neighbor classification. Pattern recognition, 35(10), 2311-2318.

Table and Figure captions

Figure 1 Study area, Northern Italy; in red the 209 polygons used for calibration, cross validation and testing; in orange the rectangles of Sentinel 2 tiles. Image prepared using Google Earth Pro Landsat/Copernicus @2020 GeoBasis-DE/BKG US Dept of State Geographer @2020 Google.

Figure 2 Classification results using three algorithms (BGLM = Bayesian Generalized Linear Model; KNN = K-Nearest Neighbor; RF = Random Forests) with four sets of predictors as input (Set 1 = Sentinel 2 bands; Set 2 = Sentinel 2 vegetation indices; Set 3 = Sentinel 1 post event data; Set 4 = Sentinel 1 pre-post event difference data). The models were validated with a 9-fold cross validation approach.

Table 1. List of vegetation indices used for tests.

	Vis	Index name	Bands
1	NDVI_idx	Normalized Difference Veg index	(b8-b4)/(b8+b4)
2	NBr_idx	Normalized Burn Ratio	(b8 – b12)/(b8 + b12)
3	NDVI_2	Normalized Difference Veg index 2	(b12-b8)/(b12+b8)
4	SR	Simple Ratio	b8/b4
5	ARI1	Anthocyanin Reflectance Index 1 (ARI1)	1/b3-1/b5
6	EVI	Enhanced Vegetation Index	2.5*(b8−b4)/(b8+ 6*b4−7.5*b2)+1000
7	NDMI	Normal difference moisture index	(b8−b11)/(b8+b11)
8	MSI	Moisture soil index	b11/b8
9	BAI	Burn Area Index	$1/(0.1\text{-b4})^2 +(0.06\text{-b8})^2$
10	DVI	Difference Veg Index	b8-b4
11	GDVI	Green Difference Vegetation Index	b8 – b3
12	GARI	Green Atmospherically Resistant Index	b8-(b3- (b2-b4)/b8+(b3- (b2-b4)
13	GRVI	Green Ratio Vegetation Index	b8/b3
14	IPVI	Infrared Percentage Vegetation Index	b8/b8+b4

Table 2. Set of S2 and S1 predictors used in classification models.

Set	**Predictors**	**Image date**
S2_Set1	Sentinel 2 (post event) bands	28/06/2019
S2_Set2	Sentinel 2 (post event) Vegetation Indices	28/06/2019
S1_Set3	Sentinel 1 (post event) bands VH, VV	07-15/12/2018
	Sentinel 1 (post event) band ratios VV/VH, VH/VV	07-15/12/2018
	Sentinel 1 (post event) normalized difference VV-VH, VH-VV	07-15/12/2018
S1_Set4	Sentinel 1 (pre-post event difference) bands VH, VV	26/09- 03/10/2018 07-15/12/2018
	Sentinel 1 (post event difference) band ratios VV/VH, VH/VV	26/09- 03/10/2018 07-15/12/2018
	Sentinel 1 (pre-post event difference) normalized difference VV-VH, VH-VV	26/09- 03/10/2018 07-15/12/2018

Table 3. Overall accuracy for classification models validated with 9-fold cross validation (OA*cv*), with related standard deviation *sd*(OA*cv*) and best hyperparameters combination. The highest Accuracy for each model is shown in bold.

		Best hyperparameters		**9-fold-cross validation**	
BGLM	***Predictors set***			**OA$_{cv}$**	***sd*(OA$_{cv}$)**
	S2_Set1			0.80	0.086
	S2_Set2			**0.82**	0.073
	S1_Set3			0.68	0.072
	S1_Set4			0.67	0.096
KNN		***kmax***	***Distance***		
	S2_Set1	15	2	0.82	0.081
	S2_Set2	20	1	**0.85**	0.102
	S1_Set3	53	2	0.71	0.138
	S1_Set4	12	2	0.66	0.085
RF		***Max. features***	***Max. depth***		
	S2_Set1	4	11	0.83	0.070
	S2_Set2	8	27	**0.84**	0.064
	S1_Set3	3	40	0.66	0.075
	S1_Set4	4	35	0.66	0.089

736

737 **Table 4**. Accuracy statistics for the three classification models and the four set of predictors
738 obtained on the Test set (10% of samples). In bold the highest OA obtained.

	Predictor set	Overall accuracy	Producers accuracy Healthy forest %	Producers accuracy Damaged areas %	Users accuracy Healthy forest %	Users accuracy Damaged areas %
BGLM	S2_Set1	0.77	87.50	71.43	63.64	90.91
	S2_Set2	**0.82**	100.00	73.33	63.64	100.00
	S1_Set3	0.50	50.00	50.00	27.27	72.73
	S1_Set4	0.55	54.55	54.55	54.55	54.55
KNN	S2_Set1	**0.86**	100.00	78.57	72.73	100.00
	S2_Set2	0.82	88.89	76.92	72.73	90.91
	S1_Set3	0.50	50.00	50.00	45.45	54.55
	S1_Set4	0.64	61.54	66.67	72.73	54.55
RF	S2_Set1	0.82	88.89	76.92	72.73	90.91
	S2_Set2	**0.86**	90.00	83.33	81.82	90.91
	S1_Set3	0.64	63.64	63.64	63.64	63.64
	S1_Set4	0.68	64.29	75.00	81.82	54.55

739

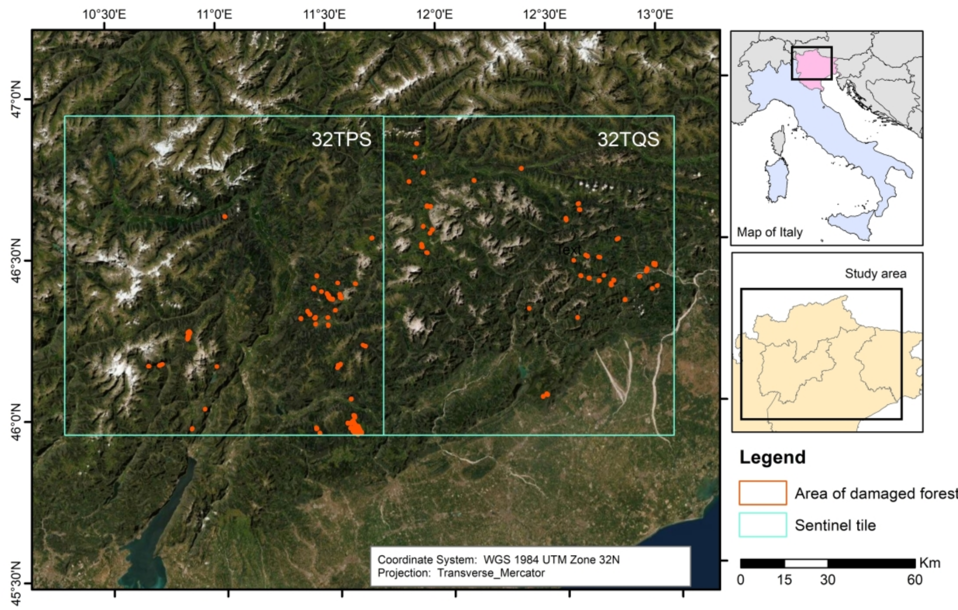

Study area, Northern Italy; in red the 209 polygons used for calibration, cross validation and testing; in orange the rectangles of Sentinel 2 tiles. Image prepared using Google Earth Pro Landsat/Copernicus @2020 GeoBasis-DE/BKG US Dept of State Geographer @2020 Google.

248x175mm (300 x 300 DPI)

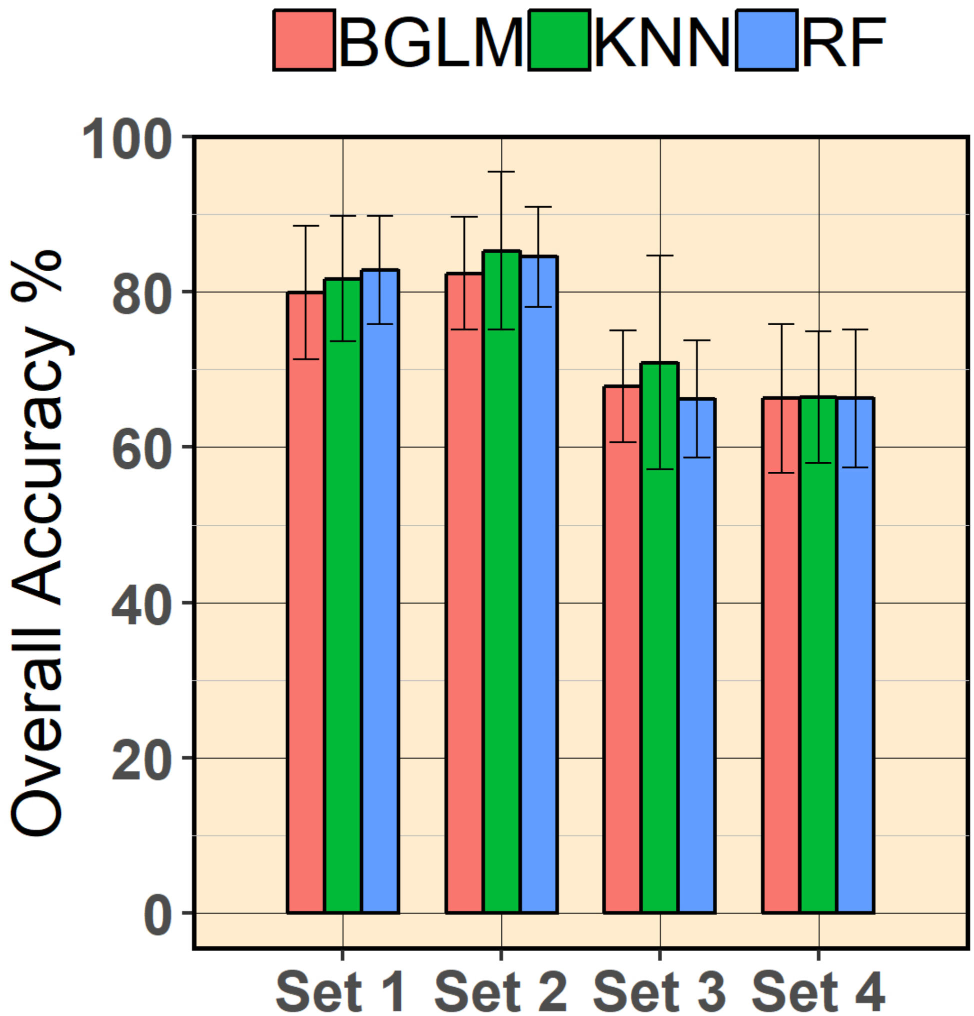

Classification results using three algorithms (BGLM = Bayesian Generalized Linear Model; KNN = K-Nearest Neighbor; RF = Random Forests) with four sets of predictors as input (Set 1 = Sentinel 2 bands; Set 2 = Sentinel 2 vegetation indices; Set 3 = Sentinel 1 post event data; Set 4 = Sentinel 1 pre-post event difference data). The models were validated with a 9-fold cross validation approach.

Response to reviewer #2

Many thanks for the positive evaluation of this revised version. We implemented the minor suggested changes as follows:

L 137-156: please revise: Revision has been made

L 358-360: please revise: Revision has been made

Figure 1: The figure has been improved and the polygons are now well visible.

Forestry *An International Journal of Forest Research*

Satellite open data to monitor forest damage caused by extreme climate-induced events: a case study of the Vaia storm in Northern Italy

Gaia Vaglio Laurin[1*], Saverio Francini[2,5], Tania Luti[3], Gherardo Chirici[2], Francesco Pirotti[4], Dario Papale[1]

[1]*Department for Innovation in Biological, Agro-Food and Forest Systems, University of Tuscia, Viterbo, 01100, Italy*

[2]*Department of Agricultural, Food and Forestry Systems, Università degli Studi di Firenze, Firenze, 50145, Italy*

[3]*Department of Earth Science, Università degli Studi di Firenze, Firenze, 50121, Italy*

[4]*Interdepartmental Research Center of Geomatics (CIRGEO), University of Padova, Legnaro, 35020, Italy*

[5]*Dipartimento di Bioscienze e Territorio, Università degli Studi del Molise, Pesche, Isernia, Italy*

*Corresponding author: Tel: +39 0761 357394; Fax: +39 0761 357389; Email: gaia.vl@unitus.it

The ~~occurrence~~frequency of ~~strong storms~~extreme storm events has significantly increased in the past decades, causing significant damage to European forests. To mitigate the impacts of extreme events a rapid assessment of forest damage is crucial, and satellite data are an optimal candidate for this task. The integration of satellite data in the operational phase of monitoring ~~of~~ forest damage can be ~~promoted exploiting~~exploit the complementarity of optical and Synthetic Aperture Radar open datasets from the Copernicus ~~free of cost datasets~~programme. This study illustrates the testing of Sentinel 1 and Sentinel 2 data for the detection of areas impacted by the Vaia storm in Northern Italy. The use of multispectral Sentinel 2 provided the best performance, with classification Overall Accuracy values up to 86%; however optical data use are seriously hampered by cloud cover that can persist for months after the event and in most cases cannot be considered an appropriate tool if a fast response is required. The results obtained using Synthetic Aperture Radar Sentinel 1 were slightly less accurate (Overall Accuracy up to 68%), but the method

was able to provide valuable information rapidly, mainly because the acquisition of this dataset is weather independent. Overall, for a fast assessment Sentinel 1 is the better of the two methods where multispectral and ground data are able to further refine the initial SAR-based assessment.

Introduction

In recent years, extreme climate-induced events have caused significant damage to European forests. The occurrence of strong storms has significantly increased in the past decades (Usbeck et al. 2010), and the frequency of these events is expected to increase ~~even more~~further in future years due to ~~the~~ changing climate dynamics (Saadet al. 2017; Seidl et al. 2014). ~~Windthrown is~~Windthrow has a major ~~driver of~~impact on forest dynamics. Forests affected by repeated damage may not have enough time to recover and are ~~exposed~~more vulnerable to ~~additional impacts.~~other threats. The ~~regrowth~~forest regeneration in areas damaged by storms can alter the overall ecosystem succession, with consequences on biodiversity (Ellison et al. 2005). The way in which the windthrown timber is managed ~~also~~ has an impact on biodiversity (Duelli et al. 2019). After a storm, the fungal infections over deadwood can increase and expand, promoting stand degradation (McCarthy et al. 2012); similarly, the expansion of outbreaks of bark beetles ~~outbreaks~~ from damaged to healthy stands, that commonly occur from one to three years after windthrow, is known to additionally impact conifer forests (Havašová et al. 2017). Civil security issues can also be very relevant in windthrow areas (Gardiner et al. 2010).

~~For operational planning, fast intervention,~~Rapid assessment of forest damage is crucial for decision support regarding actions to be taken to prevent further damage and to mitigate the impacts of future extreme events~~, a rapid assessment of forest damage is crucial.~~. Field operations ~~conducted in a timely way by~~are commonly the first response from forest authorities ~~are fundamental~~ for human security, ~~for~~ timber management, and ~~for~~ ecosystem conservation. The planning and execution of forest operations ~~needs to take~~ takes advantage ~~of~~from the availability of rapid information~~, locating the most~~ regarding spatial characteristics of the strongly impacted sites and also regarding the extent and severity of damage~~, also considering the difficulty to work in~~. Accessibility of remote forest areas is also a key factor that influences efforts that are required to collect this type of data. Remote sensing (RS) has frequently been employed to monitor different forest hazards and it has been previously used also in the case of ~~withdrawn damage~~the detection of storm-damaged trees. Various RS data can be used for post-event forest damage assessment, each having specific advantages and disadvantages, with their selection driven by site characteristics, imagery and resources availability, and the question being answered (Schwarz et al. 2003). Several case studies are needed, considering the variety of instruments and environmental conditions, to understand how to better support the integration of remote sensing tools in forest management practice.

With airborne or UAVs surveys, very detailed information up to single tree level can be produced using digital cameras (Duan et al. 2017; Hamdi et al. 2019; Honkavaara et al. 2013; Mokroš et al. 2017; Pirotti et al. 2016), or laser scanning instruments (Marchi et al. 2017; Chirici et al. 2018), or commercial multispectral sensors (Jackson et al. 2000). But on~~-~~-demand airborne or UAVs surveys are costly, suited for areas of limited extent, and flights can be hampered for weeks after the event by bad weather conditions, such as heavy rain or post-fire smoke. ~~As natural~~Natural hazards ~~are usually phenomena affecting~~often affect large areas and ~~causing~~cause diffuse impacts, consequently the mapping and monitoring of ~~damage~~the area can take advantage of the use of data from satellite platforms, that can cover broad extents repeatedly in time (Poursanidis and Chrysoulakis 2017). For this purpose, on-demand multispectral satellite images at very high spatial resolution (< 5 m) were previously successfully used in Russian (Kislov et al. 2020), and in German forests (Einzmann et al. 2017; Schwarz et al. 2003). Several forest damage assessments were conducted using medium spatial resolution multispectral data, particularly the Landsat open archive that offers free data at 30 m pixel size. As an example, with Landsat data an old diffusive windthrow caused by a storm was detected in a French forest by Haidu et al. (2019); disturbance due to intensive harvesting and strong windthrow was mapped in Western Siberia forests by Dyukarev et al. (2011); damage caused by a wind storm were assessed in Lithuania forests by Jonikavičius and Mozgeris (2013); windthrow disturbance was mapped in the temperate forest zone of European Russia and the southern boreal forest zone of the United States by Baumann et al. (2014~~); and recently~~). Recently, a Pan-European mapping of windthrow was generated through a model based on Landsat images, plus ancillary forest data from other satellites and national inventory data (Pecchi et al. 2019). Overall, optical-based studies have demonstrated the feasibility of detecting windthrow in forests using satellite images and that the accuracy of results depends mainly on the spatial and spectral resolutions of the datasets. However, the use of optical data for the rapid assessment of forest windthrows is not encouraged due to different factors, including the purchase cost and time in the case of on-demand images, and, importantly, the presence of clouds that in most cases persists for weeks after weather-related events and hamper the use of satellite data.

To cope with these limits, the use of Synthetic Aperture Radar (SAR) satellite data ~~is~~are recommended for a ~~fast~~faster response~~, it is daylight and weather~~. SAR data are independent ~~data, that in principle are~~ from solar illumination and weather. They are therefore available ~~soon~~right after the event only depending on the revisit time of the carrier, even when adverse weather conditions persist. Different SAR missions are available at present, each with specific configurations in terms of the frequency of the active signal, the polarization, and the spatial resolution. In forests, the energy backscattered by SAR systems at higher frequencies (e.g. X and C-band) mainly comes from the crowns and the upper forest strata, while at lower frequencies (e.g. L and P-bands) the contribution from branches and trunks increases, together with the signal penetration through the canopy (Solimini et al. 2016). The SAR backscatter is also influenced by the water content and the geometric features of the target object, thus in the case of forests by the moisture levels (in vegetation and soil) and the vegetation structure, including stem, branches and leaf characteristics and architecture (Woodhouse 2005). In severely damaged forest areas the geometric features suddenly change, as well as the surface roughness, making SAR data potentially suitable for forest damage assessment, and specifically for detection of windthrow (Eriksson et al. 2012). SAR datasets can bring additional and complementary information with respect to optical data (e.g. on canopy roughness, water content, and volume) (Green 1998). Few studies proved the value of SAR data in the context of detection of forest windthrows including: a multisensor based research conducted by Schwarz et al. (2003), who compared the results obtained with SAR data against those from optical data; the detection of areas affected by wind and insect outbreaks performed with L-band data (Tanase et al. 2018); and the detection of windthrow in Germany and Switzerland based on Sentinel 1 C-band data (Rüetschi et al. 2019).

Considering the different characteristics of satellite data, their integration into operational forest monitoring after extreme events seeks to exploit the complementary features of optical and SAR data. At present, this is feasible using the Copernicus European satellite ~~facilities~~missions, specifically the Sentinel 1 C-band SAR data and the Sentinel 2 optical multispectral data (Drusch et al. 2012; Torres et al. 2012). More relevant, these datasets are also available as preprocessed products in Google Earth Engine (GEE), an integrated platform designed to empower not only traditional remote sensing scientists but also a wider audience with limited technical image processing skills (Gorelick et al. 2017). With its dense time series of optical and SAR data provided free, already preprocessed, the Copernicus datasets represent an optimal tool for the rapid assessment of land processes, including large scale forest damage and windthrow, as in this specific case study.

The Vaia storm hit the North-Eastern part of Italy on the 29th October 2018; with winds exceeding 200 km/h and strong rainfall it caused extensive forest damage in 494 municipalities, destroying or severely damaging forests of about 42,500 ha, with an estimated stock of fallen trees of 85 million of cubic metres (Chirici et el. 2019). The Copernicus Emergency Mapping system reports only about 4000 ha of damaged areas, about 10% of the affected area, due to cloud cover presence in the optical images used for mapping (data available at: https://emergency.copernicus.eu/mapping/list-of-components/EMSR334). Following the Vaia storm, the impacted regions assessed the forest damage by means of the integration of aerial photographs or very high-resolution optical satellite images with data from field surveys.

The present research ~~examines the testing of~~tests Sentinel 1 and Sentinel 2 data for the detection of areas impacted by the Vaia storm. ~~Different algorithms were exploited for the classification of~~To classify healthy and damaged areas, different algorithms were evaluated , including a Bayesian Generalized Linear Model, a k-Nearest Neighbors approach, and Random Forest, using ground ~~truthing~~data provided by the regional authorities for model calibration and validation. ~~With respect to sensors~~Change detection approaches based on pre and post event image differencing were frequently used in previous ~~studies,~~research (Dalponte et al. 2020; Ruetschi et al. 2019; Tanase et al. 2018). In this work we evaluated the impact of algorithm selection on results, to support the selection of proper methods in operational forest monitoring. The present research expands on the ~~classical~~common monitoring of forest windthrow ~~monitoring~~ based on optical data, which is ineffective in case of adverse atmospheric conditions, and it introduces testing of Sentinel 1 SAR C-band~~;~~

~~furthermore,~~. Sentinel 2 optical data are here tested for the first time, according to our knowledge~~.~~, in the context of the detection of forest damages by storms. Even if the sensitivity of SAR signal to forest ~~damage~~damages was previously illustrated by various authors (Eriksson et al. 2012; Thiele et al. 2012; Ulander et al. 2005), only very few studies exploited SAR for windthrow mapping (Ruetschi et al. 2019; Tanase et al. 2018), possibly due to data complexities and limited access to user-friendly processing tools. Thus, the present study can be of help to understand how SAR can support forestry practice, also considering that these data and related tools are increasingly available by different space agencies, and preprocessed ~~S1 datasets are delivered by GEE. With respect to algorithms, change detection approaches based on pre and post event image differencing were frequently used in previous research (Dalponte et al. 2020; Ruetschi et al. 2019; Tanase et al. 2018). Here we experimented with three different supervised classification algorithms, evaluating the impact of algorithm choice on results, to provided additional knowledge that can guide the selection of proper methods in operational forest monitoring.~~Sentinel 1 datasets are delivered by GEE.

The aim of this research is to contribute to forestry practice, developing knowledge useful to operational management to exploit ~~freely available~~ satellite open-data, and defining a strategy for the rapid detection of forest damage and the further refinement of information. Remote sensing has great potential to cost-efficiently map storm-affected regions, but previous research has been somewhat limited, as Sentinel 2 imagery was not previously exploited with this aim; and Sentinel 1 was only partially examined. Thus, ~~more studies are needed~~further investigation to ~~translate~~assess the ~~remote sensing~~ potential of integrating satellite open-data into ~~actual practice.~~forest practical workflows is needed. Here the focus is on open-data from the Copernicus ~~free data, preprocessed in~~programme, exploiting the GEE platform for ~~easiness of application,~~fast processing, demonstrating that ~~demonstrates to be an optimal choice for the~~this approach can significantly support decision makers with remote sensing-based assessment of windthrow damaged areas.

Methods

Study area and ground data

The research was conducted in Northern Italy, in areas affected by the windthrow and included in two selected Sentinel-2 tiles for which ground truth data were made available by local administrations encompassing three regions: Friuli Venezia Giulia, Trentino Alto Adige, and Veneto (fig. 1). These regions host important forest resources, and different local agencies in charge of their census and management were involved in assessing the Vaia impacts. These data can also by found in open databases (Forzieri et al. 2020).

Insert fig.1

For the Trentino Alto Adige region, ground data for the Trento Autonomous Province were provided by the local forest service, and for the Autonomous Province of Bozen by the Province authority; in both cases the area of damaged forest were detected on the basis of photointerpretation of aerial orthophotos, and integrated with data from field surveys. Overall, in Trentino Alto Adige there were 1463 discrete areas, covering 5913 ha, and with a mean area of 4 ha. For the Friuli Venezia Giulia region, ground data on forest damage were provided by the local forest service using aerial orthophotos and ground surveys; there were 499 damaged areas for this region, covering 3693 ha, with mean area of 7.4 ha. For the Veneto region, the ground data were provided by the Veneto Agency for agriculture payments (AVEPA), who are responsible to provide economic help in case of natural disasters. AVEPA provided a shapefile of the affected areas based on photointerpretation of very high resolution orthophotos (20 cm spatial resolution) and SPOT 6/7 satellite pre and post event images at 1.5 m spatial resolution. The dataset included information on ~~perimeters~~area borders and estimation of percentage of damaged trees in each area. In total, there were 1588 damaged areas detected in Veneto, covering 4020 ha, and having a mean surface of ~~-~~2.5 ha.

The data provided for these Italian regions ~~were~~included 3550 polygons that identify any area affected by the windthrow ~~with an area greater than X.X ha~~. These polygons were filtered out to create a subset for testing and validation purposes, according to the following inclusion criteria: (i) polygons >2 ha, to include areas compatible with the spatial resolution and the detection capability of the remote sensing data used in this study; (ii) polygons in which the average terrain slope was below 20% in at least 85% of the surface, to exclude areas of unreliable SAR signal, according to distortion; (iii) for the Veneto region only, polygons in which the amount of damaged trees resulted > 80~~% (representing >~~%, that were more than 40% of the total Veneto polygons~~)~~;; (iv) polygons included in two Sentinel tiles, to test the methods in the most affected area (3218 polygons). For classification purposes, polygons in forest not impacted by the Vaia storm were also drawn in proximity of the impacted polygons, by on-screen photointerpretation of post-event Google ~~Earth~~ imagery.

In particular, the first criterion was guided by the imagery spatial resolution and allowed to retain the larger damaged areas. The second criterion was derived after exploring the SAR distortion masks based on local incidence angle. These maps are a by-product of SAR data processing, that was additionally performed as these layers are not included in the GEE available datasets~~; the~~. The maps indicated frequent distortions above the 20% slope~~:~~, to facilitate the analysis using GEE data, this single threshold was selected. The third criterion was applied in Veneto, and was introduced due to the different ways the Italian regions assessed damage. In fact, it was noted that ~~in~~ Trentino and Friuli Venezia Giulia ~~assessed~~ reported only areas ~~were the mostly highly impacted~~where damage was very significant, while ~~in~~ Veneto Region also digitized areas that were partially impacted ~~were included in the census, that reported the damage percentage. Retaining~~. The dataset was standardized by keeping only the polygons with damage ~~>~~degree above 80% in Veneto ~~allowed to standardize the dataset among regions, according to visual inspection of forest cover in Google Earth imagery~~. The application of the mentioned criteria resulted in a standardized dataset including the larger and most affected areas, where SAR data ~~were robust and~~ had the higher signal to noise ratio and the forest impacts were similar. The ~~damage~~damaged and ~~undamage~~non-damaged datasets included a total of 209 polygons, 104 from healthy forest stands, and 105 from damaged forest areas; the corresponding pixels were extracted from the imagery and averaged at polygon level. In total 90% of the 209 polygons ~~(187, namely the calibration dataset)~~ were used to calibrate and validate with the k-fold approach classification algorithms. The remaining 22 polygons were used as independent test set for ~~double~~further evaluation of the overall accuracy. The total area used for calibration, validation and testing the methods was considerable: in Trentino Alto Adige it was equal to 622 ha; in Veneto to 533 ha; and in Friuli 237 ha, representing the different forest types and environmental conditions occurring in the area of interest.

Copernicus Sentinel data

The Sentinel 2 (S2) multispectral images were downloaded from Google Earth Engine as Level-2A orthorectified atmospherically corrected surface reflectance. The S2 Multispectral Instrument (MSI) samples 13 spectral bands: visible and NIR at 10 meters, red edge and SWIR at 20 meters, and atmospheric bands at 60 meters spatial resolution. Only bands at 10 - 20 m spatial resolution were used for tests (bands # 2, 3, 4, 5, 6, 7, 8, 8A, 11, 12), resampling at 10 m the 20 m bands with a nearest neighbor approach. The vegetation indices included in Table 1 were also computed.

Insert Table 1

To evaluate the hypothesis ~~concerning the ability of~~that Sentinel 2 data ~~to correctly~~can detect the damaged forest areas with significant accuracy, post-event Sentinel 2 images were used. The possibility to use also a pre-damage image and focus the analysis on the variations in reflectance was also evaluated, but confounding factors such as day-specific atmospheric conditions, including cloud cover, and plant phenology stage at different dates were considered ~~important~~relevant causes of increased uncertainty in results and leading to uncertainty. Therefore, we preferred to work only on post-damage optical images using a binary classification approach (healthy forest/damaged areas).

The first available post-event Sentinel 2 imagery is dated June 2019 (7 months after the event). The predictor set named S2_Set1 (set of image bands) was used to evaluate the contribution of ~~bands~~each single band, and the S2_Set2 (vegetation indices) ~~contributed~~to evaluate the contribution of the derived vegetation indices~~, that~~. The latter combination is preferable in case ~~of usage of multiple~~different images ~~is preferred~~are used (predictor sets in Table 2).

The Sentinel 1 SAR images were downloaded from Google Earth Engine as Ground Range Detected (GRD) scenes, already pre-processed using the Sentinel-1 Toolbox to generate a calibrated, ortho-corrected product at 10 m spatial resolution in dual-band cross polarization mode (VV – VH). Preprocessing included thermal noise removal, radiometric calibration, and terrain correction using a digital terrain model (SRTM 30 m). Five pre-event scenes were collected from the period 26 September - 3 October 2018 (pre-event period without frost or snow), and 5 post-event scenes were from the period 7 - 15 December 2018. The pre and post event scenes were averaged at pixel level, and band ratios (VV/VH, VH/VV), and band normalized differences were also computed (VV-VH, VH -VV). In fact, with respect to the optical images, the SAR data are less affected by atmospheric condition and vegetation phenology and for this reason the use of differences between pre and post event was also evaluated to detect forest damaged areas.

Thus, the set of predictors named S1_Set3 (based only on post-event bands), and the S1_Set4 (based on pre-post event scenes differences) were used in tests (predictor sets in Table 2).

Insert Table 2

Classification approaches

Three different approaches were tested for the classification task: a generalized linear Bayesian model and two machine learning models, the k-Nearest Neighbors and Random Forest. Using the three models and the four sets of available predictors (Table 2), a total of 12 models-predictors combinations were developed. The tests were conducted using the RFTrainer, KNN, and Bayesglm R packages in R environment (R Core Team 2013).

Bayesian inference is a method of statistical inference in which Bayes' theorem is used to update the probability for a hypothesis as more evidence or information becomes available. It facilitates representing and taking full account of the uncertainties related to models and parameter values. The Bayesian generalized linear model (BGLM) is based on Bayesian functions that finds an approximate posterior mode and variance using extensions of the classical generalized linear model computations. The Bayesian function allows the user to specify independent prior distributions for the coefficients in the t family, with the default being Cauchy distributions with center 0 and scale set to 10 (for the regression intercept), 2.5 (for binary predictors), or 2.5/(2 · sd), where sd is the standard deviation of the predictor in the data (for other numerical predictors) (Berrett and Calder 2016; Gelman et al. 2008)

The k-Nearest Neighbors (KNN) technique is a popular method for producing spatially contiguous predictions of forest attributes by combining field and remotely sensed data. KNN are appealing as they can be used for both univariate and multivariate prediction, no assumptions regarding the distributions of response or auxiliary variables are necessary and they can be used with a wide variety of datasets (Chirici et al 2016). The k nearest vectors, used to perform the classification, are found according to Minkowski distance and the classification is performed by means of the maximum of summed kernel densities; both ordinal and continuous variables can be predicted (Wu et al. 2002).

Random Forest (RF) is an ensemble of decision trees that learns through a supervised approach and produces multiple models that are aggregated, using a bootstrap aggregating procedure, to produce the result. The models are built using different training subsets, generated by bootstrapping, that are used to build the "forest". RF is able to reduce the output variance and the overfitting problem with respect to other machine learning approaches, improving model stability and accuracy (Breiman 2001).

When a model is ~~fit~~trained with data there is ~~always~~ the risk of overfitting, i.e. that the parameters are estimated to reproduce closely the ~~examples~~training data used, losing the capacity to generalize outside the calibration examples. To avoid overfitting one of the most useful method is k-fold cross validation (k-fold CV) that ~~further~~ splits the training set into K number of subsets, called folds: the models are then iteratively fitted K times each time training the data on data from K-1 of the folds and evaluating the performances on data from the Kth fold. At the end of calibration~~-~~, the performance on each of the K folds are evaluated in term of Overall Accuracy (OA), i.e. the percentage of cases where the classification as damaged or not damaged was correct. The Overall Accuracy from Cross Validation ~~Overall Accuracy-~~ OA_{cv} and the relative standard deviation $sd(OA_{cv})$ are finally computed averaging the K folds and calculating their standard deviation. This provides more information over how stable the model is by testing it over multiple sets of data.

RF and kNN models require the calibration of hyperparameters~~, here performed~~. The hyperparameters are calculated using the training ~~polygons~~datasets. BGLM instead does not require hyperparameters calibration. A procedure based on a random search grid was used for the optimization (Bergstra and Bengio, 2012). The procedure defines a grid of hyperparameter ranges, as those defined above~~; 100~~. One hundred combinations were randomly sampled from the grid and for each combination a k-Fold CV was performed. For both KNN and RF the optimal hyperparameters combination with the greater OA_{cv} was finally selected. In the RF case, the hyperparameters that were tuned ~~includes~~include the maximum depth of each tree (max_depth) in the forest and the number of features (max_features) considered by each tree when splitting a node. The number of trees in the forest was set equal to 400, while the minimum number of samples required to split an internal node was set equal to 1.
In the kNN case the three hyperparameters that were optimized are: the number of neighbours considered (k), the Minkosky distance, and the kernel to use. The max_features ranged between 2 and n, where n equals the number of predictors used in input; the max_depth ranges between 1 and 40. k ranged between 1 and 60, the Minkosky distance was equal to the Euclidean and Manhattan distances, and the kernel to use were Unweighted, Weighted, Inverse, Reciprocal.

The models, once optimized and validated with k-fold approach, were further independently evaluated in terms of accuracy using the test set that includes 10% of the polygons never used during the optimization procedure. For the evaluation of the classification results, different statistics are reported, including overall accuracy, users accuracy, producers accuracy, and the percentage of omission and commission errors. User's accuracy represents how reliable the classification is in terms of actually finding damage in the real world over an area that was classified as “damaged” in the map. Producer's accuracy reports how often a damage that is found in the real world is reported in the final classified map (Cohen 1968; Congalton 1991).

Results

In table 3 we present for each model and for each of the four sets of predictors the averaged OA_{cv} obtained with a 9-fold cross validation procedure and the related standard deviation obtained averaging the different iterations. For the KNN and RF models the best hyperparameters combination, identified using a RandomSearch algorithm are also presented.

Insert Table 3

The results in Table 3, also graphically shown in fig. 2, show consistency in different models, with negligible differences among the considered approaches and limited variance from different iterations.

The best results are obtained with S2 images, with OA_{cv} always > 0.8 and included in the 0.8-0.85 range for either bands or vegetation indices, with the latter reaching a slightly higher accuracy. The standard deviation values resulted were always small with a maximum value of 0.102. This confirms the ability of S2 to detect impacted forest areas.

Lower accuracy results –in the 0.6-0.7 OA_{cv} range- are obtained when using SAR data with a slightly better scores obtained when using the S1_Set3, that includes only data from post-event scene.

Insert fig. 2

The three models were also applied to the independent test set (n = 22) to evaluate their final performance on new and unseen data and the results are shown in Table 4.

Insert Table 4

The results obtained using the independent test set are similar to those obtained with 9-fold CV but span, as expected, over a slightly higher range~~, as expected~~ considering the limited number of samples in the test set (n=22).

For sets 1 and 2, based on S2 data, the accuracy is included in the 0.77-0.86 range, and is similar across the three different models. For sets 3 and 4, based on S1 data, the accuracy range is 0.5-0.68, with higher results obtained using Random Forest model.

Overall, results in Table 4 confirm the higher accuracies obtained with the use of Sentinel 2 data with respect to those obtained with SAR data.

Discussion

The availability of satellite open~~ and~~ data that is also partly preprocessed ~~satellite data is crucial for~~ adds significant value to the procedure of the assessment of forest damages, from windthrow~~, as well as of~~ or other ~~forest~~sources of damage~~, allowing~~ that change the landscape. The final product is a classified damage map that supports rapid responses in terms of forest management~~ response. Overall, the~~. The results ~~shown~~indicate that data from the Copernicus Sentinel 1 and 2 ~~datasets~~missions are suited for the detection of damaged forest areas. SAR is especially useful for a ~~preliminary~~fast evaluation ~~aimed at fast intervention and~~, providing useful information for immediate~~-~~/short-term response actions for risk mitigation. Sentinel 2 can be used to refine the SAR initial information unless post event data are immediately available. The use of cloud-based platforms like Google Earth Engine ~~resulted an optimal choice, allowing the user to avoid~~ helps to reduce the ~~long and often complex~~ time that operators need for image download and standard pre-processing ~~of~~. A pre-defined workflow over ready-to-use imagery~~, and providing data~~ can avoid requiring highly skilled operators for processing imagery. The workflow can be partly automatic, providing maps useful to multiple end-users, even those less familiar with image processing techniques.

~~Overall, focusing~~Focusing on applications, the present research suggests that the sequential use of GEE Sentinel 1 and 2 data for better windthrow information provision is an optimal combination. Specifically, the testing of the different predictors from S1 and S2 data provided useful insights on the advantages and limits of these datasets.

The best detection of the forest areas impacted by the Vaia storm is always obtained using Sentinel 2 images. Using a 9-fold cross validation approach and either S2 bands or vegetation indices as input, the obtained overall accuracies were > 80%, with limited differences among modeling approaches, low variance from iterations, and results included in the 80-85% range. The use of vegetation indices with KNN and RF approaches provided the higher OA_{CV} values, equal to 85 and 84 %, respectively.

Very similar results are obtained when the parameterized models were validated against the independent test set, represented by 22 samples not used to calibrate the models. The obtained results, although the number of test samples is relatively low, are in a very similar OA range (77- 86%) compared with those reported for 9-fold cross validation. The highest OA score (86%) is obtained either using S2 bands with KNN model or using VIs with Random Forest. ~~From the user's perspective, thus considering how often a given class predicted by the model will actually be present on the ground, over 90% of the damaged areas were correctly classified in the different S2-based tests. From the producer's perspective, thus considering how often the real features on the ground are correctly classified by the model, damaged areas accuracy is in the 71-83% range, with higher scores obtained with RF and VIs.~~ User accuracies were over 90% whereas producer's accuracies were in the 71-83% range, with higher scores obtained with RF and VIs. This indicates that commission errors where lower then omission errors, in other words some damaged areas where not correctly detected by the classifier, thus leaving out some areas from the final map, but most of the areas classified as damaged where really damaged. It might be due to canopy of felled trees still significantly showing in the image, or also reflectance from water vapor, that commonly rises in the morning in mountainous areas, mixing with the reflectance values from the tree trunks.

It should be considered that the post-event S2 imagery employed in the study were from a single date and about 7 months after the Vaia event. The time gap between the storm and the

S2 imagery allows the greening of the ground in damaged areas, from herbal and shrubs vegetation regrowth that can produce a change in reflectance values and a consequent negative impact in the classification accuracy. The results are however in line with what has been already found in the past with Landsat data, thus at 30 m spatial resolution (30 m): an OA equal to 86% was reached in the detection of windthrows in Voges mountains in France (Haidu et al. 2019); in European Russia and United States the OA was about 75%, with more accurate results reported for larger areas (Baumann et al. 2014); and with an automatic algorithm based on Landsat time series, historical disturbance from windthrow and logging was detected in United States forest with an accuracy about 80%. According to our knowledge, there are no studies based on the use of S2 data for forest windthrow detection, except two abstracts where the accuracy of the obtained results is not reported (Cenci et al. 2019; Valt et al. 2019).

Vegetation indices are especially useful when multiple images are used (as in the case of change detection analysis), or when the study area is large and covered by different image tiles, or even when a mosaic from different dates is composed to mitigate cloud cover issues. In fact, VIs are designed to maximize sensitivity to the vegetation characteristics while minimizing confounding factors such as soil background reflectance, directional, or atmospheric effects, that change among different acquisitions (Fang and Liang 2008). According to this and based on the reported classification results, the use of VIs from S2 data, fitting the model with the RF ~~model approach~~method, appears the best solution to detect damaged forest area in this case study. An improvement in accuracy is expected if optical imagery ~~become~~becomes available in dates close to the time of the damage event.

The use of SAR inputs produced lower accuracies compared to S2 inputs with an OA values in the range 0.66-0.71 according to 9-fold cross validation and a low standard deviation score (< 0.14). Differences among the three models are minor, as well as those when using post-event data only or pre-post event backscattering difference. The highest ~~OA_{CV}~~OA_{cv} score is obtained with pre-event data and KNN approach (~~OA~~OA_{cv} = 0.71).

According to results from the independent test set, the OAs slightly decrease and the variability in values increases, being included in the 0.5-0.68 range. The best scores are obtained using RF: 64% and 68% in OA with post-event data and pre-post event difference, respectively. With RF, the user's accuracy is low (54%) when using S1 pre-post event scenes differences, but the producer's accuracy is in line with the one obtained using the S2 data (75%). When using post-event data, the user's and producer's accuracies are on the same order (63%). The results suggest the use of RF as classification model, and the combination of pre- and post-event SAR scenes to better meet the user's needs.

Previous studies conducted with C-band ERS 1/2 and RADARSAT 1 at 30 m spatial resolution were not successful for the detection of forest windthrows (Schwarz et al. 2003; Ulander et al. 2005). However, with L-band data - that better penetrates into the forest - OAs included in the 69-84% range were obtained in the Bavarian Forest National Park, with accuracy values depending on the acquisition date and environmental conditions (Tanase et al. 2018). Using C-band S1 and a change detection approach, the producer's accuracy reached 88% in a German validation site, but the user's accuracy was quite low (21~~%).~~%) and limitations consisted in a minimum area of 0.5 ha and the requirement of 10 post-event images (Rüetschi et al. 2019). Positive results were also obtained using X-band data with very high spatial resolution (Thiele et al. 2012).

The results here presented outline the relevance of SAR spatial resolution for forest windthrow detection, and confirm the ability of S1 data to produce fast preliminary information on impacted areas, with the obtained OA and user's accuracy included in a range of values similar to those reported by other studies.

It is important to note ~~that there are~~ the limitations ~~in~~of the present study~~.~~ in terms of suitability in certain cases. First, the ~~application of the models to~~ areas tested were all above 2 ha, to cope with the 10 m spatial resolution of both S1 and S2 datasets; however the average size of damaged areas in the three considered regions resulted higher than 2 ha. Then, the ground truth was filtered out to exclude slopes using a low threshold (> 20°) where the first SAR distortion effects were observed. Producing the distortion masks to filter out data, instead of a fixed threshold that excluded most slopes for easiness of analysis in GEE, could results in a detailed mapping of unreliable SAR pixels and a larger availability of ~~good~~reliable data over slopes. Similarly, the use of temporal series can improve the amount of area with reliable SAR data, as at each pass the acquisition angle may ~~change~~vary. When SAR data are used, it is also important to ~~evaluate the presence of~~ detect and mask pixels with wet or dry snow over the canopy, as it ~~impacts~~changes the ~~backscattering~~backscatter values (Koskinen et al. 1997). This implies ~~that~~an added complexity of the method in areas seasonally covered by ~~wet~~ snow ~~a data quality assessment has to be performed in certain periods~~.

~~This study aimed at a first evaluation of GEE Copernicus S1 and S2 data for windthrow monitoring, to facilitate remote sensing data exploitation in applied forestry.~~ For future operational use, the application of a pre-disturbance forest/non-forest map can help to perform semi-automatic classification. Further tests are also needed to understand the response of satellite data over less impacted forests, where a mixture of healthy and damaged trees is present, and how to minimize the impact of SAR distortion areas.

The combined use of S1 and S2 was not investigated here, as for data integration the optical and radar imagery ~~shall~~should be from same period. ~~In~~The S2 images used in this investigation were dated months after the storm, when the herbal and ~~shrubs~~shrub vegetation ~~regrowth~~renovation influence both the optical reflectance and the backscattering in C-band SAR~~: too many~~. These are confounding factors ~~would have been present~~, but a data integration approach is feasible if optical data are available soon after the event. Higher accuracy in classification is known to occur from combining SAR –with optical ~~joined use~~ with respect to use single ~~datasets use~~sensor type (Clerici et al. 2017; Vaglio Laurin et al. 2012), so this might be another strategy to improve the information accuracy.

Conclusion

This study showed the suitability of ~~GEE~~ Copernicus S1 and S2 data for the detection of areas affected by windthrow. Sentinel 2 provided the best performance for detection of windthrow areas, but its use was seriously hampered by cloud cover. For events occurring in winter, Sentinel 2 data might only be available after several months. In those cases, the use of Sentinel 1 data, being independent with respect to atmospheric condition and with a fast return time, becomes the best option for a first and rapid evaluation of the forest damage, to support field operations and the formation of management response plans.

Thus, for operational monitoring, the results suggest a sequential approach, based initially on S1 for fast response. This initial SAR assessment can be refined in later dates, integrating S2 imagery when available and data from ground or aerial surveys, for a more accurate mapping also over steep slopes.

~~X~~

Data availability statement

Remote sensing data are freely available by the Copernicus facilities. Ground data were provided by local authorities and can be requested directly to them. Part of the data can be found in the open database published by Forzieri et al. (2020).

Funding

This work was supported by internal resources of the participating institutes. In particular F.P.'s work was supported by University of Padova's VAIA-FRONT (VAIA, FROm lessons learNT to future options) project.

Acknowledgements

For the Trentino Autonomous Province, we acknowledge Dr. A. Wolynski from the local forest service who coordinated the acquisition of ground data on the basis of aerial photography and field surveys.

For the Alto Adige region, we acknowledge Dr. F. Maistrelli from the Autonoumous Province of Bozen who provided the ground data delimitated on the basis of aerial photography and field surveys.

For the Friuli Venezia Giulia region, we acknowledge Dr. R. Comino from the local forest service who coordinated the acquisition of ground data on the basis of aerial photography and ground surveys.

For the Veneto Region we acknowledge the Agenzia Veneta per i Pagamenti in Agricoltura (AVEPA) that provided the ~~ground~~ data.

Conflict of interest statement

'None declared.'

References

Baumann, M.; Ozdogan, M.; Wolter, P.T.; Krylov, A.; Vladimirova, N.; Radeloff, V.C. (2014) Landsat remote sensing of forest windfall disturbance. Remote Sens. Environ., 143, 171–179.

Bergstra, J., & Bengio, Y. (2012). Random search for hyper-parameter optimization. Journal of machine learning research, 13, 281-305.

Berrett, C., & Calder, C. A. (2016). Bayesian spatial binary classification. Spatial Statistics, 16, 72-102.

Breiman, L. (2001). Random forests. Machine learning, 45(1), 5-32.

Cenci, L., De Giorgi, A., Squicciarino, G., Pulvirenti, L., Moser, G., & Boni, G. (2019). Exploiting Sentinel 2 data for mapping windstorm damages in forested areas. Case Study: the event of October 2018 occurred in Northeast Italy. *Geophysical Research Abstracts*, vol. 21.

Chirici, G., Mura, M., McInerney, D., Py, N., Tomppo, E. O., Waser, L. T., ... & McRoberts, R. E. (2016). A meta-analysis and review of the literature on the k-Nearest Neighbors technique for forestry applications that use remotely sensed data. Remote Sensing of Environment, 176, 282-294.

Chirici, G., Bottalico, F., Giannetti, F., Del Perugia, B., Travaglini, D., Nocentini, S., ... & Fattorini, L. (2018). Assessing forest windthrow damage using single-date, post-event airborne laser scanning data. Forestry: An International Journal of Forest Research, 91(1), 27-37.

Chirici, G., Giannetti, F., Travaglini, D., Nocentini, S., Francini, S., D'Amico, G., ... & Tonner, J. (2019). Stima dei danni della tempesta "Vaia" alle foreste in Italia. Forest@-Journal of Silviculture and Forest Ecology, 16(1), 3.

Clerici, N., Valbuena Calderón, C. A., & Posada, J. M. (2017). Fusion of Sentinel-1A and Sentinel-2A data for land cover mapping: a case study in the lower Magdalena region, Colombia. Journal of Maps, *13*(2), 718-726.

Cohen, J. (1968) Weighted kappa: Nominal scale agreement with provision for scaled disagreement or partial credit. Psychological Bulletin 70 (4):213-220.

Congalton, R.G. (1991) A review of assessing the accuracy of classification of remotely sensed data. Remote Sensing of Environment 37:35-46

Dalponte, M., Marzini, S., Solano-Correa, Y. T., Tonon, G., Vescovo, L., & Gianelle, D. (2020). Mapping forest windthrows using high spatial resolution multispectral satellite images. International Journal of Applied Earth Observation and Geoinformation, 93, 102206.

Drusch, M., Del Bello, U., Carlier, S., Colin, O., Fernandez, V., Gascon, F., ... & Meygret, A. (2012) Sentinel-2: ESA's optical high-resolution mission for GMES operational services. Remote sensing of Environment, 120, 25-36.

Duan, F.; Wan, Y.; Deng, L. (2017) A novel approach for coarse-to-fine windthrown tree extraction based on unmanned aerial vehicle images. Remote Sens., 9, 306.

Duelli, P., Wermelinger, B., Moretti, M., & Obrist, M. K. (2019). Fire and windthrow in forests: Winners and losers in Neuropterida and Mecoptera. Alpine Entomology, 3, 39.

Dyukarev, E.A.; Pologova, N.N.; Golovatskaya, E.A.; Dyukarev, A.G. (2011) Forest cover disturbances in the South Taiga ofWest Siberia. Environ. Res. Lett., 68.

Einzmann, K., Immitzer, M., Böck, S., Bauer, O., Schmitt, A., & Atzberger, C. (2017) Windthrow detection in European forests with very high-resolution optical data. Forests, 8(1), 21.

Ellison, A. M. et al. (2005) Loss of foundation species: Consequences for the structure and dynamics of forested ecosystems. Front. Ecol. Environ. 3, 479–486.

Eriksson, L.E.B.; Fransson, J.E.S.; Soja, M.J.; Santoro, M. (2012) Backscatter signatures of wind-thrown forest in satellite SAR images. In Proceedings of the International Geoscience and Remote Sensing Symposium (IGARSS), Munich, Germany, 22–27 July; pp. 6435–6438.

Fang H. and S. Liang. (2008) Leaf Area Index Models. Encyclopedia of Ecology, pp. 2139-2148

Forzieri, G., Pecchi, M., Girardello, M., Mauri, A., Klaus, M., Nikolov, C., … Beck, P. S. A. (2020). A spatially explicit database of wind disturbances in European forests over the period 2000 - 2018. Earth System Science Data, 12(1), 257–276.

Gardiner, B., Blennow, K., Carnus, J. M., Fleischer, P., Ingemarsson, F., Landmann, G., ... & Peyron, J. L. (2010). Destructive storms in European forests: past and forthcoming impacts. European Forest Institute, Efiatlantic.

Gelman, A., Jakulin, A., Pittau, M. G., & Su, Y. S. (2008) A weakly informative default prior distribution for logistic and other regression models. The annals of applied statistics, 2(4), 1360-1383.

Gorelick, N., Hancher, M., Dixon, M., Ilyushchenko, S., Thau, D., & Moore, R. (2017) Google Earth Engine: Planetary-scale geospatial analysis for everyone. Remote sensing of Environment, 202, 18-27.

Green, R.M. (1998) The sensitivity of SAR backscatter to forest windthrow gaps. Int. J. Remote Sens., 19, 2419–2425.

Haidu, I., Furtuna, P. R., & Lebaut, S. (2019) Detection of old scattered windthrow using low cost resources. The case of Storm Xynthia in the Vosges Mountains, 28 February 2010. Open Geosciences, 11(1), 492-504.

Hamdi, Z. M., Brandmeier, M., & Straub, C. (2019) Forest Damage Assessment Using Deep Learning on High Resolution Remote Sensing Data. Remote Sensing, 11(17), 1976.

Havašová, M., Ferenčík, J., & Jakuš, R. (2017) Interactions between windthrow, bark beetles and forest management in the Tatra national parks. Forest Ecology and Management, 391, 349-361.

Honkavaara, E.; Litkey, P.; Nurminen, K. (2013) Automatic Storm Damage Detection in Forests Using High-Altitude. Photogrammetric Imagery. Remote Sens., 5, 1405–1424.

Huang, C., Goward, S. N., Masek, J. G., Thomas, N., Zhu, Z., & Vogelmann, J. E. (2010) An automated approach for reconstructing recent forest disturbance history using dense Landsat time series stacks. Remote Sensing of Environment, 114(1), 183-198.

Jackson, R. G., Foody, G. M., & Quine, C. P. (2000) Characterizing windthrown gaps from fine spatial resolution remotely sensed data. Forest Ecology and Management, 135(1-3), 253-260.

Jonikavičius, D., & Mozgeris, G. (2013) Rapid assessment of wind storm-caused forest damage using satellite images and stand-wise forest inventory data. iForest-Biogeosciences and Forestry, 6(3), 150.

Kislov, D. E., & Korznikov, K. A. (2020) Automatic Windthrow Detection Using Very-High-Resolution Satellite Imagery and Deep Learning. Remote Sensing, 12(7), 1145.

Koskinen, J.T.; Pulliainen, J.T.; Hallikainen, M.T. (1997) The Use of ERS-1 SAR Data in Snow Melt Monitoring. IEEE Trans. Geosci. Remote Sens. 35, 601–610.

Marchi, N., Pirotti, F., & Lingua, E. (2018). Airborne and Terrestrial Laser Scanning Data for the Assessment of Standing and Lying Deadwood: Current Situation and New Perspectives. Remote Sensing, 10(9), 1356.

McCarthy, J. K., Hood, I. A., Kimberley, M. O., Didham, R. K., Bakys, R., Fleet, K. R., ... & Brockerhoff, E. G. (2012) Effects of season and region on sapstain and wood degrade following simulated storm damage in Pinus radiata plantations. Forest ecology and management, 277, 81-89.

Mokroš, M.; Výbošt'ok, J.; Merganicˇ, J.; Hollaus,M.; Barton, I.; Korenˇ ,M.; Tomaštík, J.; Cˇ ernˇava, J. (2017) Early stage forest windthrow estimation based on unmanned aircraft system imagery. Forests 8, 306.

Pecchi, M., Forzieri, G., Ceccherini, G., Spinoni, J., Feyen, L., Cescatti, A., & Chirici, G. (2019) Pan-European mapping of windthrows. Geophysical Research Abstracts, vol. 21.

Pirotti, F., Travaglini, D., Giannetti, F., Kutchartt, E., Bottalico, F., & Chirici, G. (2016). Kernel feature cross-correlation for unsupervised quantification of damage from windthrow in forests. ISPRS - International Archives of the Photogrammetry, Remote Sensing and Spatial Information Sciences, XLI-B7, 17–22.

Poursanidis, D., & Chrysoulakis, N. (2017) Remote Sensing, natural hazards and the contribution of ESA Sentinels missions. Remote Sensing Applications: Society and Environment, 6, 25-38.

R Core Team (2013). R: A language and environment for statistical computing. R Foundation for Statistical Computing, Vienna, Austria. URL http://www.R-project.org/.

Rüetschi, M., Small, D., & Waser, L. T. (2019) Rapid detection of windthrows using sentinel-1 c-band sar data. Remote Sensing, *11*(2), 115.

Saad, C., Boulanger, Y., Beaudet, M., Gachon, P., Ruel, J. C., & Gauthier, S. (2017) Potential impact of climate change on the risk of windthrow in eastern Canada's forests. Climatic Change, 143(3-4), 487-501.

Schwarz, M., Steinmeier, C., Holecz, F., Stebler, O., & Wagner, H. (2003) Detection of windthrow in mountainous regions with different remote sensing data and classification methods. Scandinavian journal of forest research, 18(6), 525-536.

Seidl, R., Schelhaas, M. J., Rammer, W., & Verkerk, P. J. (2014) Increasing forest disturbances in Europe and their impact on carbon storage. Nature climate change, 4(9), 806-810.

Solimini, D. (2016) Understanding Earth Observation; Springer International Publishing: Basel, Switzerland, pp. 1–703, ISBN 978-3-319-25633-7.

Tanase, M. A., Aponte, C., Mermoz, S., Bouvet, A., Le Toan, T., & Heurich, M. (2018) Detection of windthrows and insect outbreaks by L-band SAR: A case study in the Bavarian Forest National Park. Remote Sensing of Environment, 209, 700-711.

Thiele, A., Boldt, M., & Hinz, S. (2012) Automated detection of storm damage in forest areas by analyzing TerraSAR-X data. In: 2012 IEEE International Geoscience and Remote Sensing Symposium (pp. 1672-1675). IEEE.

Torres, R.; Snoeij, P.; Geudtner, D.; Bibby, D.; Davidson, M.; Attema, E.; Potin, P.; Rommen, B.Ö.; Floury, N.; Brown, M.; et al. (2012) GMES Sentinel-1 mission. Remote Sens. Environ., 120, 9–24.

Ulander, L.M.H.; Smith, G.; Eriksson, L.; Folkesson, K.; Fransson, J.E.S.; Gustavsson, A.; Hallberg, B.; Joyce, S.; Magnusson, M.; Olsson, H.; et al. (2005) Mapping of wind-thrown forests in southern Sweden using space- and airborne SAR. In Proceedings of the International Geoscience and Remote Sensing Symposium (IGARSS), Seoul, South Korea, 25–29 July 2005; pp. 3619–3622.

Usbeck, T., Wohlgemuth, T., Dobbertin, M., Pfister, C., Bürgi, A., & Rebetez, M. (2010). Increasing storm damage to forests in Switzerland from 1858 to 2007. Agricultural and Forest Meteorology, 150(1), 47-55.

Vaglio Laurin, G., Liesenberg, V., Chen, Q., Guerriero, L., Del Frate, F., Bartolini, A., ... & Valentini, R. (2013) Optical and SAR sensor synergies for forest and land cover mapping in a tropical site in West Africa. International Journal of Applied Earth Observation and Geoinformation, 21, 7-16.

Valt, M., Salvatori, R., & Salzano, R. (2019) Mapping the effects of VAIA storm using Sentinel 2 data. *Geophysical Research Abstracts,* vol. 21.

Woodhouse, I. H. (2005). Introduction to microwave remote sensing. CRC press.

Wu, Y., Ianakiev, K., & Govindaraju, V. (2002) Improved k-nearest neighbor classification. Pattern recognition, 35(10), 2311-2318.

Table and Figure captions

Figure 1 Study area, Northern Italy; in red the 209 polygons used for calibration, cross validation and testing; in orange the rectangles of Sentinel 2 tiles. Image prepared using Google Earth Pro Landsat/Copernicus @2020 GeoBasis-DE/BKG US Dept of State Geographer @2020 Google.

Figure 2 Classification results using three algorithms (BGLM = Bayesian Generalized Linear Model; KNN = K-Nearest Neighbor; RF = Random Forests) with four sets of predictors as input (Set 1 = Sentinel 2 bands; Set 2 = Sentinel 2 vegetation indices; Set 3 = Sentinel 1 post event data; Set 4 = Sentinel 1 pre-post event difference data). The models were validated with a 9-fold cross validation approach.

Table 1. List of vegetation indices used for tests.

	Vis	**Index name**	**Bands**
1	NDVI_idx	Normalized Difference Veg index	(b8-b4)/(b8+b4)
2	NBr_idx	Normalized Burn Ratio	(b8 – b12)/(b8 + b12)
3	NDVI_2	Normalized Difference Veg index 2	(b12-b8)/(b12+b8)
4	SR	Simple Ratio	b8/b4
5	ARI1	Anthocyanin Reflectance Index 1 (ARI1)	1/b3-1/b5
6	EVI	Enhanced Vegetation Index	2.5*(b8−b4)/(b8+ 6*b4−7.5*b2)+1000
7	NDMI	Normal difference moisture index	(b8−b11)/(b8+b11)
8	MSI	Moisture soil index	b11/b8
9	BAI	Burn Area Index	$1/(0.1-b4)^2 +(0.06-b8)^2$
10	DVI	Difference Veg Index	b8-b4
11	GDVI	Green Difference Vegetation Index	b8 – b3
12	GARI	Green Atmospherically Resistant Index	b8-(b3- (b2-b4)/b8+(b3- (b2-b4)
13	GRVI	Green Ratio Vegetation Index	b8/b3
14	IPVI	Infrared Percentage Vegetation Index	b8/b8+b4

Table 2. Set of S2 and S1 predictors used in classification models.

Set	Predictors	Image date
S2_Set1	Sentinel 2 (post event) bands	28/06/2019
S2_Set2	Sentinel 2 (post event) Vegetation Indices	28/06/2019
S1_Set3	Sentinel 1 (post event) bands VH, VV	07-15/12/2018
	Sentinel 1 (post event) band ratios VV/VH, VH/VV	07-15/12/2018
	Sentinel 1 (post event) normalized difference VV-VH, VH-VV	07-15/12/2018
S1_Set4	Sentinel 1 (pre-post event difference) bands VH, VV	26/09- 03/10/2018 07-15/12/2018
	Sentinel 1 (post event difference) band ratios VV/VH, VH/VV	26/09- 03/10/2018 07-15/12/2018
	Sentinel 1 (pre-post event difference) normalized difference VV-VH, VH-VV	26/09- 03/10/2018 07-15/12/2018

Table 3. Overall accuracy for classification models validated with 9-fold cross validation (OA*cv*), with related standard deviation *sd*(OA*cv*) and best hyperparameters combination. The highest Accuracy for each model is shown in bold.

		Best hyperparameters		**9-fold-cross validation**	
BGLM	***Predictors set***			**OA_{cv}**	***sd*(OA_{cv})**
	S2_Set1			0.80	0.086
	S2_Set2			**0.82**	0.073
	S1_Set3			0.68	0.072
	S1_Set4			0.67	0.096
KNN		***kmax***	***Distance***		
	S2_Set1	15	2	0.82	0.081
	S2_Set2	20	1	**0.85**	0.102
	S1_Set3	53	2	0.71	0.138
	S1_Set4	12	2	0.66	0.085
RF		***Max. features***	***Max. depth***		
	S2_Set1	4	11	0.83	0.070
	S2_Set2	8	27	**0.84**	0.064
	S1_Set3	3	40	0.66	0.075
	S1_Set4	4	35	0.66	0.089

778

779 **Table 4**. Accuracy statistics for the three classification models and the four set of predictors
780 obtained on the Test set (10% of samples). In bold the highest OA obtained.

	Predictor set	Overall accuracy	Producers accuracy Healthy forest %	Producers accuracy Damaged areas %	Users accuracy Healthy forest %	Users accuracy Damaged areas %
BGLM	**S2_Set1**	0.77	87.50	71.43	63.64	90.91
	S2_Set2	**0.82**	100.00	73.33	63.64	100.00
	S1_Set3	0.50	50.00	50.00	27.27	72.73
	S1_Set4	0.55	54.55	54.55	54.55	54.55
KNN	**S2_Set1**	**0.86**	100.00	78.57	72.73	100.00
	S2_Set2	0.82	88.89	76.92	72.73	90.91
	S1_Set3	0.50	50.00	50.00	45.45	54.55
	S1_Set4	0.64	61.54	66.67	72.73	54.55
RF	**S2_Set1**	0.82	88.89	76.92	72.73	90.91
	S2_Set2	**0.86**	90.00	83.33	81.82	90.91
	S1_Set3	0.64	63.64	63.64	63.64	63.64
	S1_Set4	0.68	64.29	75.00	81.82	54.55

781